J. Fluid Mech. (1981), *vol.* 111, *pp.* 233–269
Printed in Great Britain

Turbulence measurements in an adverse-pressure-gradient three-dimensional turbulent boundary layer along a circular cylinder

By H. H. FERNHOLZ AND J.-D. VAGT
Hermann-Föttinger-Institut für Thermo- und Fluidynamik,
Technische Universität Berlin

(Received 17 July 1980 and in revised form 23 December 1980)

Measurements, including the six components of the Reynolds-stress tensor, have been made along three generators of a centre-mounted circular cylinder with an elliptical nose cone. The pressure distribution was axisymmetric upstream and asymmetric downstream. The streamwise adverse pressure gradient led to almost zero skin friction in the direction of the limiting streamline, and the circumferential pressure gradient led to skew angles up to 30° in the vicinity of the wall. Special emphasis was laid on measurements in the wall region ($y^+ > 4$), on the repeatability of these measurements and on an estimate of error bounds. The turbulence level encountered (up to 60% close to the wall) was much higher than in other three-dimensional boundary-layer measurements. It has been shown that available measuring techniques have to be improved considerably or even abandoned if used under these conditions. Previous measurements of collateral velocity profiles in three-dimensional boundary layers will probably now have to be corrected for severe aerodynamic interference effects.

It has been shown that the normal stresses $\overline{u_i'^2}$ and the shear stress component $\overline{u'v'}$ behave qualitatively much as those in a two-dimensional adverse pressure-gradient boundary layer. The other components, $\overline{v'w'}$ and $\overline{u'w'}$, both characteristic of three-dimensional flow and caused by the circumferential pressure gradient, are influenced in different ways by the streamwise and circumferential pressure gradients. Spectra of u'-fluctuations are again similar to those obtained from two-dimensional boundary layers.

Mean velocity profiles obey the linear and logarithmic law of the wall known from two-dimensional boundary layers both along a line of symmetry and in the three-dimensional boundary layer. This may be because the streamwise pressure gradient dominates over the circumferential pressure gradient in this experiment.

Finally it has been found that the skew angle γ of the Reynolds shear stress vector leads the skew angle ζ of the resultant velocity gradient or 'mean shear', both having the opposite sign of the skew angle β of the mean velocity vector except close to the wall. The ratio of Reynolds shear stress and turbulent kinetic energy is no longer 'approximately' constant as is assumed for two-dimensional boundary layers.

1. Introduction

This paper describes and discusses mean-flow and turbulence measurements in a three-dimensional pressure-driven boundary layer with a strong adverse pressure gradient in the streamwise direction and a weaker lateral pressure gradient causing the boundary layer to become three-dimensional in the downstream part of the test section. Experimental data from the mean- and fluctuating-flow field are necessary to develop turbulence models for the closure of the boundary-layer equations and to serve as test cases for numerical computations of three-dimensional boundary layers. In the course of this investigation available measuring techniques were found to show serious defects due to high turbulence levels, probe interference effects and wall proximity. Improved measuring techniques in the wall region ($y^+ \leqslant 100$) of the highly turbulent boundary layer have enabled us, for example, to provide some further insight into the similarity laws of the mean velocity in the inner region ($4 \leqslant y^+ \leqslant 200$), to point out possible error sources for flow angle measurements near a wall and to present Reynolds shear-stress data close to separation.

There are several survey papers on three-dimensional boundary layers, e.g. by Eichelbrenner (1973), Fanneløp & Krogstad (1975) and Johnston (1976), and we therefore need not review investigations up to 1976 unless specifically relevant to our own measurements. Johnston presents a detailed list of those experiments in which turbulent stress profiles were measured in his table 5. We have extended this listing (including our own experiment) and present it as table 1 of this paper.

A comparison of the various investigations shows that only the experiment performed by Ezekwe, Pierce & McAllister (1978) has a similar geometry to ours and additionally that only Hebbar & Melnik (1976, 1978) have carried out measurements in the immediate vicinity of the wall. This can be seen from the values of the wall coordinate y^+.

Table 1 also gives the orientation of the stem of the hot-wire probes which is parallel, slightly inclined to the wall or normal to the wall. The latter probe arrangement is most probably superior for near-wall measurements since it is less prone to probe effects due to aerodynamic interference. This is of special importance since good mean and fluctuating velocity data are rare in the wall-layer region and since large changes of the flow angle (figure 6) and of the mean velocity (figure 8) may occur below $y^+ = 100$.

The raw data of our experiment (measuring stations are given in table 2) are published in an internal HFI report by Fernholz *et al.* (1978), while probe effects and improved measuring techniques in the near-wall region were discussed by Vagt & Fernholz (1979). This paper will henceforth be referred to as I. A detailed description of the axisymmetric upstream boundary layer was given by Fernholz & Vagt (1975).

Section 2 of this paper presents an account of the experimental arrangement and the flow regime, while §3 describes briefly the hot-wire techniques, peculiarities of the measuring techniques in general and error bounds. Section 4 provides a discussion of the measurements and §5 gives comparisons with assumptions which concern closure models or semi-empirical relations used in calculation methods.

Authors	Source and type of cross flow	Number of 3-D profiles	Measurement method for Reynolds stress data and listing of data	Technique for mean field data and skin friction measurements	Maximum flow angle† Measuring method	y^+_{min}
Dechow (1977)	Cylindrical body normal to the wall. Pressure-driven flow	14	Quarter square method, single and X-wires, stem parallel to the wall. $\overline{u'^2}, \overline{v'^2}, \overline{w'^2}, \overline{u'v'}, \overline{u'w'}, \overline{v'w'}$	Normal single hot wire. Preston probe; direction of skin friction with hot film probe	60° X-wire	—
Hebbar & Melnik (1976, 1978)	Yawed flow decaying to 2-D; flat wall	9	Single rotated hot-wire probe. Probe protruding out of the wall. $\overline{u'^2}, \overline{w'^2}, \overline{u'w'}$	Normal hot wire. Preston probe; sub-layer fence; hot film	22° Bisector method	0·31
Chandrasekhara Swamy *et al.* (1978)	20° yawed flat plate at two angles of incidence. Zero pressure gradient	more than 7	Normal single and X-wire probe. Probe stem parallel or 3° inclined towards the wall. $\overline{u'^2}, \overline{v'^2}, \overline{w'^2}, \overline{u'v'}, \overline{u'w'}, \overline{v'w'}$	Normal single hot-wire, Pitot probe. Preston probe	12° 3-hole yaw probe	~ 30
Ezekwe *et al.* (1978)	Free-jet over a flat wall impinging against a back wall. Off and on plane of symmetry	4	Rotating hot-film technique, straight and slanted hot-films. $\overline{u'^2}, \overline{v'^2}, \overline{w'^2}, \overline{u'v'}, \overline{u'w'}, \overline{v'w'}$	Straight hot film. No skin friction data	— Rotating hot film	—
De Grande & Hirsch (1978)	60° curved duct flow decaying along a straight extension; flat wall	140	Single rotated hot wire; single normal and slanted wire. Probe protruding out of the wall. $\overline{u'^2}, \overline{v'^2}, \overline{w'^2}, \overline{u'v'}, \overline{u'w'}, \overline{v'w'}$	Normal single hot wire. 3-hole probe. No skin friction measurements	28° 3-hole probe	< 10 estimate
Müller & Krause (1979); Müller (1979)	Adverse chordwise pressure gradient due to inclined side wall and upper wall	21	Single normal, slanted wire, X-probe. Stem parallel to the wall. $\overline{u'^2}, \overline{v'^2}, \overline{w'^2}, \overline{u'v'}, \overline{u'w'}, \overline{v'w'}$	Normal single hot wire. Preston probe	53° Bisector method	—
Fernholz & Vagt (1980)	Adverse pressure gradient, pressure driven circumferentially due to inclined back wall	24	Single normal, slanted and X-wire. Probe stem normal to the wall. $\overline{u'^2}, \overline{v'^2}, \overline{w'^2}, \overline{u'v'}, \overline{u'w'}, \overline{v'w'}$, u'-spectra	Normal single hot wire. Preston probe, surface fence	31° Modified rotating hot-wire	4

† against free-stream direction.

TABLE 1. Three-dimensional turbulent-boundary-layer experiments with turbulent-stress profiles.

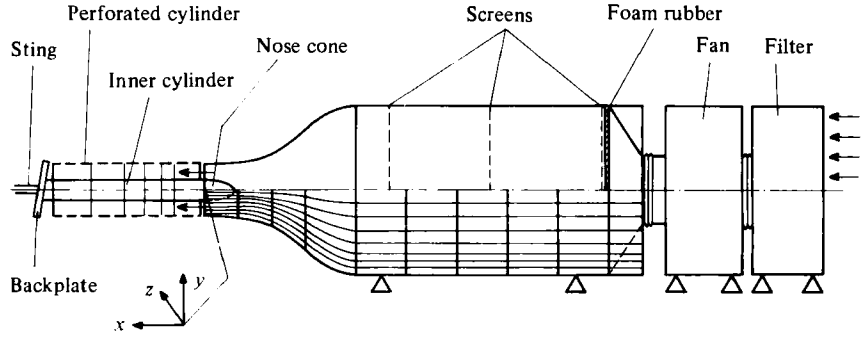

FIGURE 1. Wind tunnel and test section.

2. Experimental arrangement and flow regime

Description of the test rig and the tunnel

The wind tunnel used in this investigation was described by Vagt (1973). It is a low-speed blower tunnel with a 12 kW motor and centrifugal fan, an air-filter intake and a 2 m long settling chamber with two wire gauzes $[(1-d/l)^2 = 0{\cdot}59$, where d is the diameter of the wire and l the mesh size], and a slab of foam rubber, followed by an 11:1 axisymmetric contraction (figure 1). A carefully organized programme of screen adjustment resulted in a uniform exit velocity so that local mean velocities $\bar{u}$ across the nozzle exit varied at most by $\pm 1{\cdot}5\,\%$ with a turbulence intensity $(\overline{u'^2})^{\frac{1}{2}}/\bar{u}$ of $0{\cdot}10\,\%$ in a frequency range up to 10^4 Hz.

All measurements were performed at a test-section inlet velocity of about 18 $\mathrm{m\,s^{-1}}$ with a fixed Reynolds number $(\bar{u}/\nu)_{\mathrm{ref}} = 1{\cdot}23\times 10^6\ \mathrm{m^{-1}}$. The laboratory was air-conditioned (room temperature held constant at $22\pm 0{\cdot}5°$, or even $\pm 0{\cdot}1$ °C in special cases), in order to minimize the drift of hot wires and transducers.

The test section consisted of a sting-mounted horizontal inner cylinder (0·25 m in diameter, 1·55 m long and made of Ultramid S, a plastic material) with an elliptical nose cone 0·30 m long and a concentric perforated outer cylinder (38 % open area ratio) of 0·60 m diameter. A back plate was fitted at the downstream end of the annulus to control the width of the flow exit and the axial pressure distribution of the flow.

Pitot tubes and hot-wire probes, mounted on an electrically driven traverse gear, were introduced into the test section through a slot along a generator of the outer cylinder wall. The traverse gear provided precise linear (incremental resolution 0·005 mm) and angular (resolution 0·09 degree) movements. Surface fences, protruding approximately 0·10 mm from the surface of the inner cylinder (Vagt & Fernholz 1973), alternated with static pressure tappings (0·8 mm diameter) along one generator of the inner cylinder. By turning the inner or the outer cylinder, measurements could be made with the wall probes at fixed positions x along the circumference and with the other probes at any position in the flow field covered by a circumferential angle of about 30 degrees.

Mean and fluctuating velocities were measured using probes with single normal, slanted or X-wires. These probes were especially developed for this investigation, and operated by DFVLR (HDA III) constant-temperature anemometer units. For the measurements of flow angles the CTAs were connected to DFVLR integrators allow-

ing integration times up to 1000 s. For measurements of velocity fluctuations the anemometers were used in conjunction with a turbulence-intensity measuring device (Froebel & Vagt 1977) which provided r.m.s. values, sums, differences and divisions of signals. The signals were read into a teletype unit by means of a data transfer unit (Schlumberger DTU), connected to a digital voltmeter, punched on a paper tape and finally evaluated on an HP 1000 computer.

The hot wires were calibrated in the free stream of the test section at a position ($x = 0{\cdot}531$ m, $z = 0$) where the turbulence level was less than 0·3 % and where the velocity was constant in a range $20 < y < 140$ mm normal to the wall. The flow velocity was measured in the same plane by means of a Pitot probe (1 mm diameter) and a static pressure tapping and evaluated by an automatic micro-manometer with a resolution of 0·01 mm water column (Froebel & Vagt 1974). The hot-wire calibration was checked after each profile measurement. It turned out to be very stable as a result of the controlled conditions provided by the temperature control and the air filter.

All hot-wire probes were designed to cause as little aerodynamic interference as possible and their design and manufacturing process is described in detail by Dahm & Vagt (1977). For a single normal hot wire probe the distance between the prongs is 4 mm and their length 10 mm. The hot wire consists of a central sensitive section of platinum-coated tungsten wire, 5 μm in diameter and 1·3 mm long. The gold-plated end sections are approximately 30 μm in diameter and are soldered to the prongs, which have the same diameter at the tips as the plated wire.

Aerodynamic interference effects were checked by applying the 'rotation test' described by Comte-Bellot, Strohl & Alcaraz (1971). It was found that the mean velocity measured by the hot wire increases by 2·3 % at most in the velocity range up to 30 m s^{-1} if the probe stem is arranged normal to the flow direction, i.e. normal to the wall. Such a probe arrangement was essential if severe probe–flow interference effects were to be avoided in a flow region with strong curvature of the streamlines in the vicinity of a wall (see I). For an evaluation of near-wall measurements in three-dimensional boundary layers one must be careful to use an appropriate stem position of the hot-wire probe. Our results confirm an earlier suggestion by Bissonnette & Mellor (1974), who also used a hot-wire probe with the stem normal to the wall, 'that interference effects need not be too critical' if the hot-wire probes are properly designed.

Stem and prongs of the X-wire probe have the same size as those of the normal-wire probe. The gap between the two wires is 1 mm in order to try to minimize the thermal effects of wake interference, and the separation of the prongs is again 4 mm. An aerodynamic interference test showed that the probe signals were not seriously affected in the probe positions used in the investigation.

The slanted-wire probe used for the measurement of the Reynolds-stress component $\overline{v'w'}$ needs a more detailed discussion, which may be found in I.

Flow regime

The flow field studied in this investigation was chosen with two themes in mind: a well-understood uniform upstream boundary layer providing the starting conditions for the three-dimensional boundary layer which develops downstream and a pressure-driven three-dimensional boundary layer growing under adverse pressure gradient conditions in streamwise direction. The boundary layer intended to fulfil these

conditions was generated on the inner cylinder of the test section with the flow in the direction of the cylinder axis (figure 1).

The boundary layer along the surface of the inner cylinder was axisymmetric from the nose cone to about one third of the test-section length and three-dimensional further downstream. This was achieved by means of the backplate. By inclining this backplate so that it was no longer normal to the axis of the cylinder, the circumferential pressure distribution in the downstream half of the annulus could be made asymmetric, causing the originally axisymmetric boundary layer to become three-dimensional and, due to the adverse pressure gradient, to separate.

Before we describe the three-dimensional boundary layer, a brief discussion of the upstream axisymmetric boundary layer is appropriate. Preliminary investigations had shown that a laminar boundary layer followed by a transition region occupied this part of the test wall. There were, however, two disadvantages which resulted from the laminar/transitional boundary layer, first that the circumferential distribution of the skin friction which was used as a criterion for the uniformity of the boundary layer turned out to be rather non-uniform and secondly that the thickness of the three-dimensional boundary layer downstream was only about 30 mm. The effects of various tripping devices on the behaviour of the boundary layer were therefore investigated, resulting in a device which was effective and, at the same time, disturbed the boundary layer very little. Transition was achieved by a strip of 'Dymo tape' on which the letter V was printed at intervals of 4 mm, the apices of the V's pointing upstream. The tape was 0·40 mm thick and the overall height of a printed V was 0·65 mm. Forced transition made the subsequent turbulent boundary layer much more uniform and the results of detailed measurements of skin friction, mean velocity and fluctuating velocity distributions in the circumferential direction were reported by Fernholz & Vagt (1977). These measurements may be summarized as follows.

At $x = 0{\cdot}079$ m ($x = 0$ at the beginning of the circular cylinder), the wall-pressure distribution along the circumference is uniform and the skin-friction pattern showed variations of at most $\pm 8\,\%$ in amplitude. This was the smallest variation that could be achieved.

The 'wavelength λ' of the peaks in the skin friction distribution was between 22 and 44 mm corresponding to a range of the parameter $(\lambda u_\tau/\nu_w) \times 10^{-3}$ from 1·27 to 2·54. The amplitude of this circumferential skin friction distribution decreased and the wavelength of the 'peak and valley' pattern increased downstream.

The existence of circumferential irregularities across the boundary layer at different heights y from the wall was investigated by measuring the mean velocity $\bar{u}$ and the r.m.s value of the fluctuating component u' around the circumference at $x = 0{\cdot}13$ m. A distinct variation of both $\bar{u}$ and $(\overline{u'^2})^{\frac{1}{2}}$ occurs only in the viscous sublayer (figure 2) up to $y^+ = 10$ and this pattern correlates approximately with the skin friction distribution. The non-uniformities disappear beyond $y^+ = 25$.

These measurements show that the weak three-dimensional disturbances in the upstream boundary layer decay almost completely in the circumferential, normal and longitudinal (not shown here) directions so that the boundary layer may be assumed to be axisymmetric. The starting conditions for the following three-dimensional boundary layer can therefore be assumed to be effectively uniform.

The development of the mean velocity profiles in wall co-ordinates $u^+ = \bar{u}/u_\tau$ and

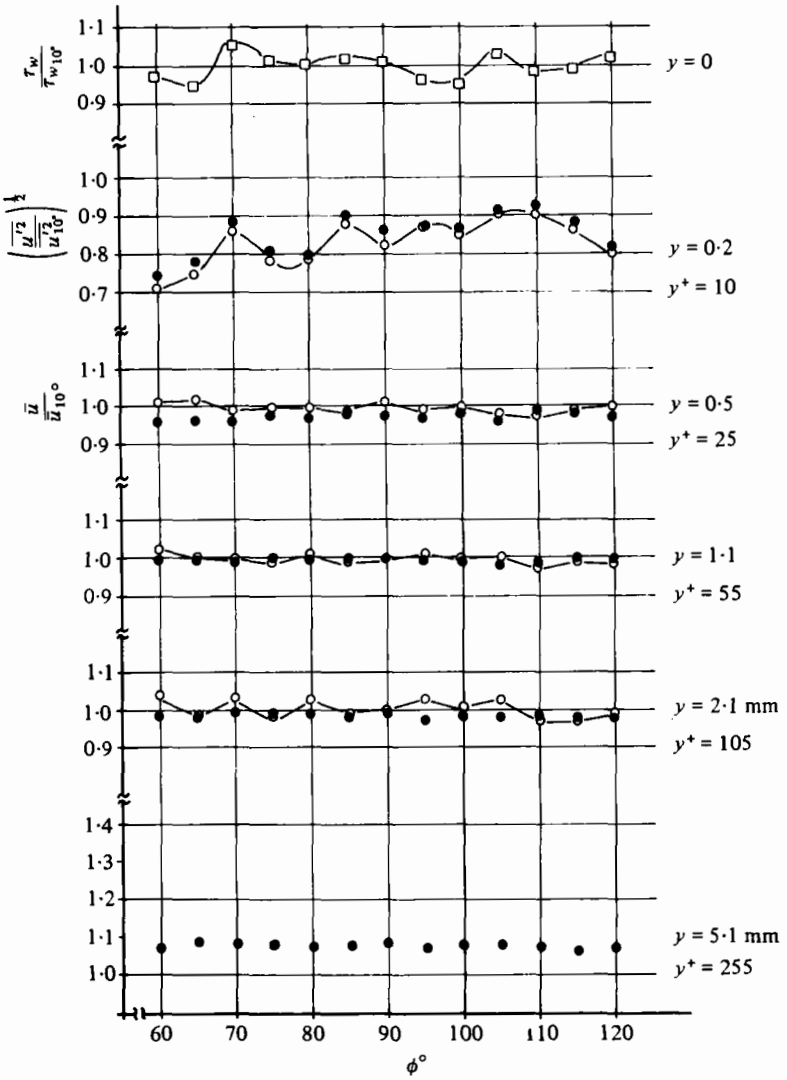

FIGURE 2. Distribution of skin friction, mean velocity and fluctuating velocity in an axisymmetric boundary layer; $x = 135$ mm; $\delta \simeq 6$ mm at $\phi = 10°$. □, $\tau_w/\tau_{w10°}$; ○, $(\overline{u'^2}/\overline{u'^2}_{10°})^{\frac{1}{2}}$; ●, $\bar{u}/\bar{u}_{10°}$.

$y^+ = u_\tau y/\nu_w$ along a generator of the cylinder ($z = 0{\cdot}0218$ m) in the axisymmetric region of the boundary layer is shown in figure 3. Here u_τ is the skin friction velocity $(\tau_w/\rho_w)^{\frac{1}{2}}$, τ_w the skin friction, ρ_w the density and ν_w the kinematic viscosity at the wall. The velocity profiles behave as is expected in a two-dimensional turbulent boundary layer. The scatter of the data is well within the measuring accuracy. The strong three-dimensionality of the boundary layer described below is therefore attributed entirely to the circumferential pressure distribution in the downstream part of the test section.

An impression of the three-dimensional flow is given in figure 4 where the flow is from left to right and where the velocity vectors are shown on three concentric planes

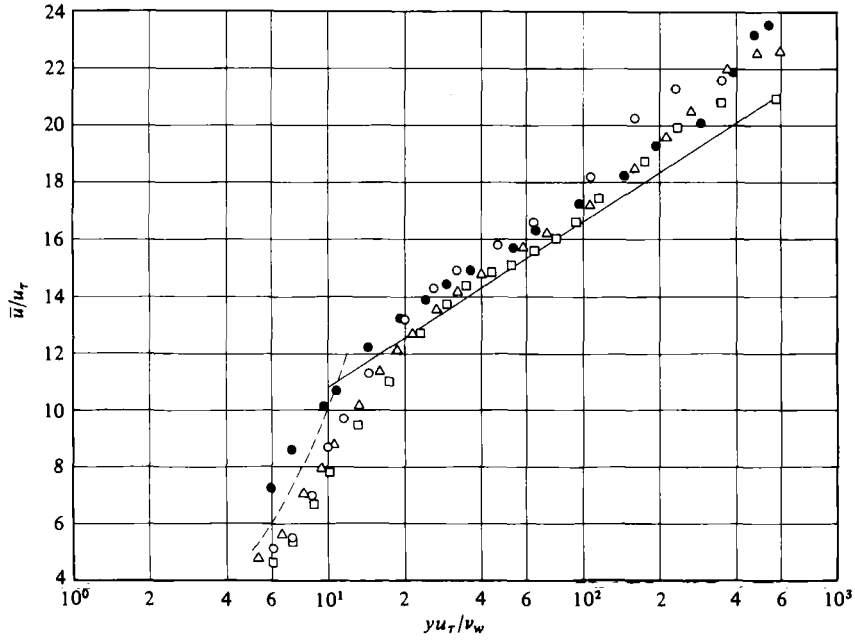

FIGURE 3. Log-law velocity profiles in an axisymmetric turbulent boundary layer at low Reynolds numbers.

Profile	x (m)	H_{12}	Re_{δ_1}
○	0·079	1·53	581
□	0·135	1·47	717
△	0·331	1·42	1271
●	0·531	1·38	1716

(y = 0·45, 5·45 mm and the outer edge) above the surface of the cylinder. Two lines of symmetry, one with flow convergence and one with flow divergence, can be observed corresponding to the widest and the narrowest part of the exit gap. The open circles indicate the separation region which is in fact a separation bubble extending downstream to the back plate. d_i and d_o denote the distance of the back plate from the inner and outer cylinder wall at the end of the test section.

The flow direction outside the boundary layer is very nearly parallel to the axis of the cylinder with a maximum angle of incidence in the xz plane of about 2 degrees (for the co-ordinate system see figure 5) and an upwash angle of at most 5° (in the xy plane).

Measurements were performed in the flow region marked by stippling in figure 4 at eight axial stations along three generators 21·8 mm apart from each other. This is the region in which the three-dimensional effects were strongest. The co-ordinates of the measuring stations, some principal flow parameters and the symbols used for the data in subsequent figures are presented in table 2 where the following definitions were used: x is the distance along a generator, z the circumferential distance from the reference generator, u_δ the free-stream velocity at the outer edge of the boundary layer, u_τ the magnitude of the skin friction velocity $(\tau_w/\rho_w)^{\frac{1}{2}}$, H_{12} the shape parameter defined as the ratio δ_1^*/Θ_{11}, β the skew angle of the mean velocity vector measured from the direction of u_δ, $\beta_{\max}$ the maximum skew angle measured, and $Re_{\Theta_{11}}$ a

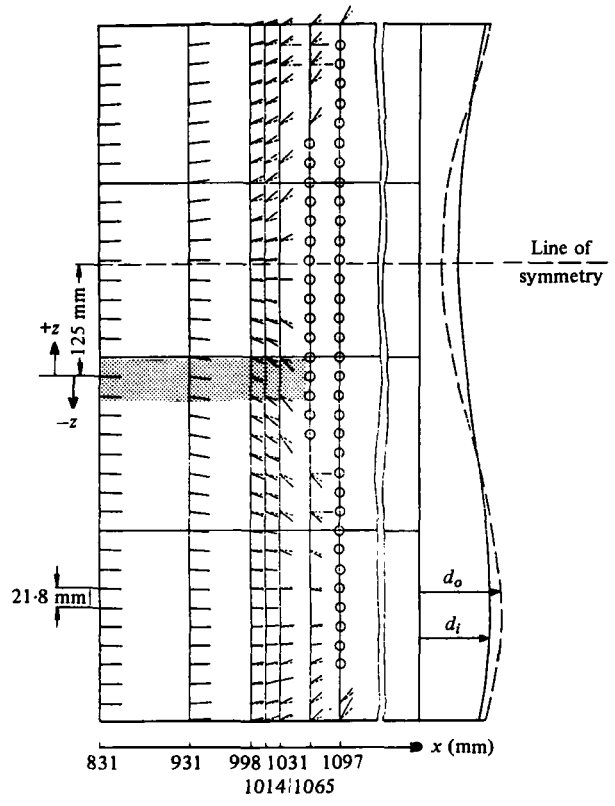

FIGURE 4. Survey of three-dimensional boundary-layer development. —·—, outer edge of boundary layer; ---, 3·45 mm; —, 0·45 mm; ○, reserve flow; ▦, measuring area.

Reynolds number defined as $\rho_\delta u_\delta \Theta_{11}/\mu_w$. The characteristic boundary-layer thicknesses are defined as

$$\delta_1^* = \int_0^\delta [1-(\bar{u}_{\mathrm{ref}}/u_\delta)]\,[1+(y/R_w)]\,dy, \tag{2.1}$$

$$\Theta_{11} = \int_0^\delta (\bar{u}_{\mathrm{ref}}/u_\delta)\,[1-(\bar{u}_{\mathrm{ref}}/u_\delta)]\,[1+(y/r_w)]\,dy, \tag{2.2}$$

with $\bar{u}_{\mathrm{ref}} = \bar{u}\cos\beta$, $\bar{u}$ being the magnitude of the local mean velocity vector and R_w the radius of the inner cylinder.

In addition, some measurements were performed along the line of symmetry (figure 4) from which streamlines diverge. Here the $\bar{w}$ component of the velocity vector is zero. These mean velocity profiles will be compared below with the axisymmetric profiles shown in figure 3 and the three-dimensional velocity profiles shown in figure 8.

Owing to the circumferential component of the pressure gradient and the transverse curvature of the wall, the mean flow and turbulence structure may be affected by combined longitudinal and transverse curvature effects in addition to three-dimensionality and adverse pressure gradient. We do not think, however, that these effects are significant since the distance over which longitudinal curvature could affect the structure of the turbulence is very short and since δ/R is well below 1.

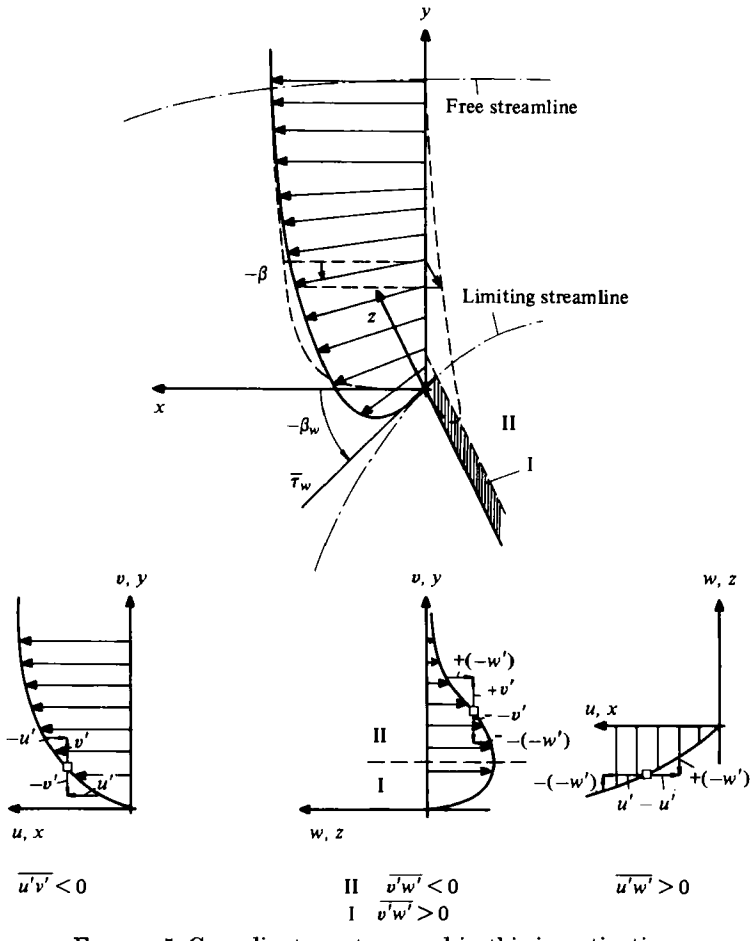

FIGURE 5. Co-ordinate system used in this investigation.

If the data should be used as a test case for computations, starting conditions are given at $x = 831$ mm for three z-positions and boundary conditions along the three generators downstream to separation at approximately $x = 1065$ mm. For the detailed tabulated data see Fernholz *et al.* (1978).

3. Measuring techniques and error bounds

In this section measuring techniques will generally be described briefly since they were reported in I and only a few aspects will be discussed in more detail as being especially relevant for some of the topics discussed in §§ 4 and 5.

Skin friction

Relying on comparative studies by Pierce & Krommenhoek (1968), McCroskey & Durbin (1972) and Hebbar & Melnik (1976), as well as on a discussion of the advantages and disadvantages of the different devices for measuring skin friction (see I),

Profile	x (mm)	u_δ (m s^{-1})	u_τ (m s^{-1})	H_{12}	$-\beta^0_{\max}$	$Re_{\Theta_{11}}$	Symbol	z (mm)
0101	531	17·95	0·7448	1·384	0	1712	◇	−21·8
0102	531	17·71	0·7434	1·403	0	1710	◆	0
0103	531	17·65	0·7417	1·435	0	1728	◇	+21·8
0201	831	16·25	0·5532	1·463	0	2957	▲	−21·8
0202	831	16·19	0·5622	1·464	0	2742	▲	0
0203	831	16·47	0·5637	1·460	3·78	3073	▲	+21·8
0301	881	15·79	0·5012	1·515	1·30	3480	■	−21·8
0302	881	15·04	0·4951	1·520	2·52	3099	■	0
0303	881	15·28	0·4898	1·517	3·30	3411	■	+21·8
0401	931	15·28	0·4242	1·602	2·15	4125	△	−21·8
0402	931	15·08	0·4337	1·580	3·63	3642	△	0
0403	931	15·02	0·4228	1·593	5·25	3823	△	+21·8
0501	964	14·47	0·3641	1·708	4·28	4414	—	−21·8
0502	964	13·59	0·3720	1·672	4·91	3542	●	0
0503	964	13·95	0·3616	1·684	8·63	4269	●	+21·8
0601	998	13·63	0·3080	1·798	6·95	4861	▨	−21·8
0602	998	13·61	0·3180	1·835	7·52	4995	□	0
0603	998	13·61	0·3137	1·799	12·62	4751	□	+21·8
0701	1031	13·30	0·2599	1·969	11·64	5822	▼	−21·8
0702	1031	13·07	0·2609	1·979	13·44	5294	▼	0
0703	1031	13·24	0·2711	2·000	22·36	5651	▼	+21·8
0801	1065	13·27	0·2270	2·166	18·52	6577	⊗	−21·8
0802	1065	13·07	0·2338	2·175	24·62	6277	○	0
0803	1065	13·08	0·2267	2·272	32·99	6499	○	+21·8

TABLE 2

we have used Preston tubes and surface fences in the three-dimensional boundary layer.

The Preston-tube method which relies on the validity of the law of the wall was further checked, though indirectly, by using two Preston tubes of different outer diameters d (0·434 and 0·890 mm). Measurements at two stations in the three-dimensional region (x = 998 and 1031 mm), where the comparison was made, agreed within $\pm 4\,\%$, the pressure difference ΔP (Preston tube signal minus static pressure) being in a range $0{\cdot}06 < \Delta P < 0{\cdot}55$ mm of water column. Since the measuring time for the smaller Preston tube was about an order of magnitude larger, the 0·89 mm tube was used for all measurements in the region downstream of x = 1014 mm. The repeatability of the measurements then lay within a bandwidth of $\pm 5\,\%$ falling to $\pm 20\,\%$ close to separation due to the very small pressure differences and the high fluctuation level of the signal (cf. figure 8).

The Preston tube was set to an average angle determined from mean flow measurements close to the wall. A more accurate adjustment has not been necessary since the sensitivity of Preston tubes to changes in flow direction is very low, within a range of $\pm 8°$. One could argue that the Preston tube disturbs the flow close to the wall by changing the flow direction. This effect does exist but we know from a comparison between surface-fence and Preston-tube measurements that the total head does not change within the above range of the flow angle.

In order to have a separate means of measuring skin friction, surface fences, the flow-angle characteristics and calibration curves of which are described by Vagt &

Fernholz (1973), were built into the curved wall. Measurements from the surface fences agreed well with the Preston-tube results over most of the boundary layer, with discrepancies ranging from 1·4 % to about 4·5 % confined to the downstream end of the boundary layer close to separation. The error bounds reported here are smaller than those in I where a mistake in the evaluation of the surface fence signals, discovered after publication, suggested a worse agreement between the two measuring techniques.

Flow angle

Flow angles were measured (for an extended description see I) by a modified version of the rotated hot-wire technique in the near-wall region, by the bisector method further out towards the edge of the boundary layer and, for comparison, by twin-tube yawmeters (cobra probes) which are probably the best of the null-reading direction probes (Dean 1953). For measurements near the wall these probes have a disadvantage resulting from their size, so that their signal gives an integral value of the flow angle and not a point measurement, and severe aerodynamic interference effects occur (see I). Twin-tube yawmeters with very small diameters need very long measuring times (for the 0·50 mm diameter probe at least 30 min), and aerodynamic interference effects close to the wall are not reduced significantly by using such small probes. Similar aerodynamic interference effects also occur when hot-wire probes are used in the near-wall region if the probe stem is inclined to the wall (Johnston (1970) used a probe inclination of about 5° for example). Such a probe arrangement gives flow angles, again close to the wall, which show a behaviour similar to that of the twin-tube yawmeter, that is the flow angle is approximately constant (figures 11 and 12 in I).

The stems of both the yawmeter and the inclined hot-wire probe affect the near-wall flow so strongly that these measurements are not representative of the actual flow, which has a much higher deflection. If the single normal hot-wire probe is however inclined by 90°, i.e. perpendicular to the wall, a monotonic increase of the flow angle is shown as the wall is approached (figure 11 in I). Such a monotonic increase in flow angle is also shown in other experiments where probe arrangements with perpendicular probe holders were employed. Rogers & Head (1969), for example, introduced a similar technique which uses a hot wire held parallel to the wall on prongs entering the flow through a rotatable wall plug.

Once aerodynamic interference effects are reduced to a minimum flow-angle measurements by means of a hot wire are usually straightforward if the flow-angle characteristic of the hot wire is symmetric, so that the bisector method can be applied. This technique may be used in flow regions not too close to a wall if the turbulence level is low ($< 20\,\%$) and if temperature changes in the flow during the measurement of the flow angle can be kept small. Figure 6 shows measurements of the flow angle along two generators of the circular cylinder. For measurements at distances from the wall greater than about $y^+ = 10$ the repeatability is $\pm 0{\cdot}5°$ in a highly turbulent flow field if the flow temperature can be controlled within a range of $\pm 0{\cdot}1$ °C. A temperature variation of 1 °C resulted in errors of up to 2° in the outer region, increasing to 4° or more closer to the wall. This is a consequence of the fact that the flow characteristic of the hot wire becomes very much flatter (figure 13 in I) and the measuring times required increase to one hour per flow angle.

Measurements below $y^+ = 20$ were therefore obtained by a modified version of the

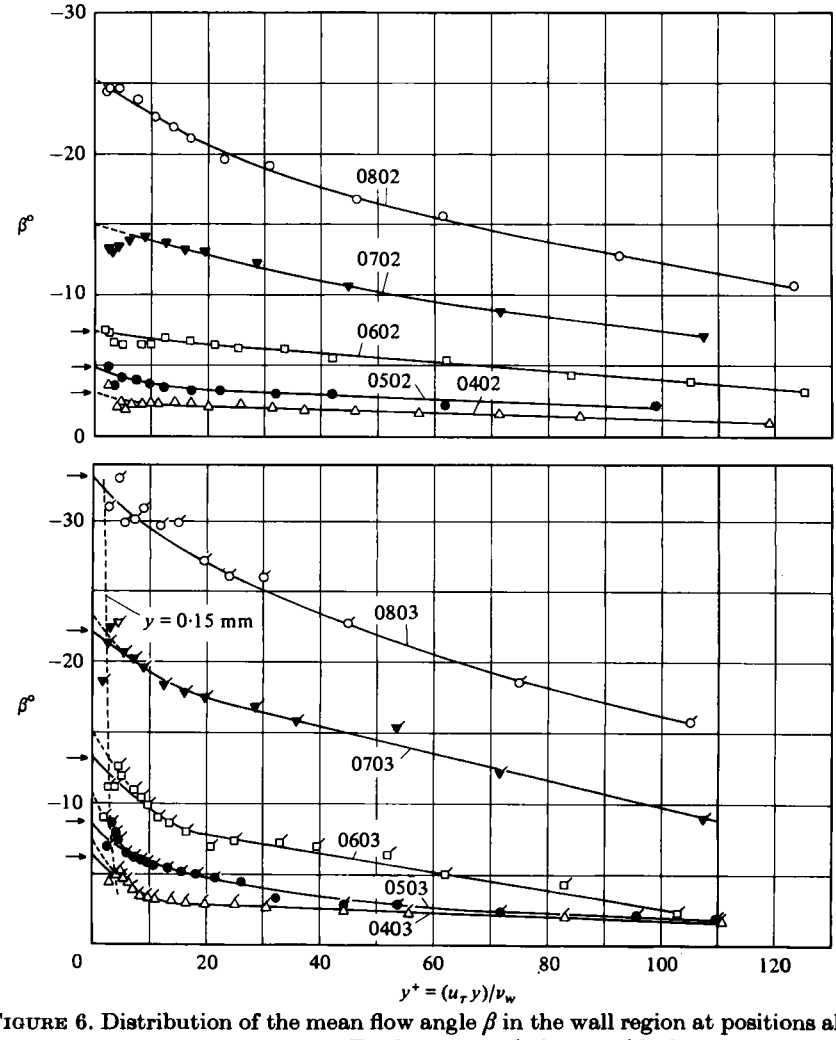

FIGURE 6. Distribution of the mean flow angle β in the wall region at positions along two generators. For key to symbols see table 2.

rotated hot-wire technique, the original version of which was suggested by Bissonnette & Mellor (1974). This technique (cf. I) reduces the measuring time to about 1 min, permits flow angle measurements closer to the wall in flow regions where velocity fluctuations are large compared to the mean velocity and/or where wall effects are severe. As with all near-wall measurements high standards of probe manufacture are required (the wire axis must be straight and parallel to the wall – in our case normal to the stem axis – and the connections between the prong tips and the wire must be carefully smoothed and polished after the soldering process). But even this technique is limited to a minimum wall distance and depends apparently on at least the magnitude of the turbulence level and the heat conductivity of the wall. As can be seen in figure 6 this limit lay at about a distance $y = 0{\cdot}15$ mm from the wall. The repeatability of the flow angle measurements in the vicinity of the wall is about $\pm 1°$, and we would claim an uncertainty of the skew angle at the wall obtained by extrapolation of about $\pm 2°$.

x (m)	$z = 2{\cdot}18 \times 10^{-2}$ m	$z = 0$ m	$z = -2{\cdot}18 \times 10^{-2}$ m
0·531	18·517	18·559	18·662
0·831	59·296	59·142	58·841
0·998	98·439	97·637	97·106
1·014	101·738	101·104	100·794
1·031	104·409	103·570	103·251
1·097	109·417	109·454	109·138

The dimensionless data tabulation is given in the report by Fernholz *et al.* (1978).

TABLE 3. Static pressure distribution $P_w - P_{ref}$ N m^{-2}.

Static pressure

Static pressure measurements at all stations along the test wall were carried out with wall static tappings consisting of 0·80 mm diameter holes drilled into 5 mm brass plugs which were flush with the surface of the wall. The plugs were connected to a strain-gauge pressure transducer (Statham PM 97 TC) or to the automatic micro-manometer referred to above. Static pressure was also measured by means of a static pressure probe (cf. Vagt & Fernholz 1977) at the outer edge of the boundary layer. Agreement was within 5%.

No static pressure measurements could be performed in the inner region of the boundary layer as a result of the high turbulence levels of $\overline{v'^2}$ and $\overline{w'^2}$ which seriously affect the signal obtained by the static pressure probe (cf. Vagt & Fernholz 1976).

Since small variations in static pressure seem to influence the results of computations considerably (Krause & Kordulla 1975) we have estimated the uncertainty of our measurement to be approximately $\pm 0{\cdot}05$ mm water, i.e. for the difference $(P_w - P_r)$ between the static pressure P_w at a fixed position and a reference pressure P_r. The pressure changes along the three generators are given in table 3. In order to show changes in static pressure with x and z we have given the data in dimensional form. Although the differences in circumferential direction are very small close to separation, they still suffice to keep the balance with the small momentum of the near-separation flow so that the deflection of the streamlines reaches its largest values there.

Mean and fluctuating velocities

Mean and fluctuating velocities were measured with single normal hot wires, with slanted hot wires, and with cross-wire probes. In the case of mean-flow measurements it is expected that the accuracy of the signals will be affected by the high level of turbulence near the separation region. Mean velocity data obtained by hot wires can be corrected by taking into account higher-order terms of the so-called wire-response equation (e.g. Vagt 1979) which, however, contains triple and quadruple correlation terms of the velocity fluctuations u' and w' which are again difficult to measure with sufficient accuracy. This means that it is still a complex operation to try to correct hot-wire signals in highly turbulent flows.

Neglecting higher-order terms in the response equation one obtains for the measured mean velocity

$$\bar{u}_{\text{measured}} = \bar{u}(1 + 0{\cdot}5\overline{v'^2}/\bar{u}^2). \tag{3.1}$$

Assuming a maximum value of $\overline{v'^2}/\tilde{u}^2 = 0{\cdot}25$ this yields a value of the velocity which is too high by 12 % in the vicinity of the wall. Such a correction would therefore bring the mean velocity measurements in the viscous sublayer and the log-law region even closer to the theoretical curves (cf. figure 8 where all data are uncorrected). Repeatability was about 1 %, and for a comparison between measurements by flattened Pitot tubes and hot-wire probes and a discussion of wall effects on the hot-wire signals, the reader is referred to I. All probes were aligned with the local flow direction as determined by a hot wire, and the normal-stress component $\overline{u'^2}$ was obtained from a single normal wire.

The normal-stress component $\overline{w'^2}$ was determined from single normal wire signals in three positions (the third normal to the flow to obtain $\overline{u'^2}$) via the relationship

$$\overline{w'^2} = (K^{-2}(\overline{e_1'^2} + \overline{e_2'^2}) - \overline{u'^2})\,(1+k)^2/(1-k)^2, \tag{3.2}$$

where e' denotes the voltage, K a calibration constant, k the yaw parameter and the indices 1 and 2 the wire inclinations in a plane parallel to the wall.

A single normal wire, set at $\pm 45°$ to the mean-flow direction, was calibrated in both orientations. The Reynolds shear stress component $\overline{u'w'}$ was then determined from the relationship

$$\overline{u'w'} = (2K^2)^{-1}\,(\overline{e_1'^2} - \overline{e_2'^2})\,(1-k^2)^{-1}. \tag{3.3}$$

The hot-wire probe was designed in such a way that the yaw parameter k was negligibly small for flow angles less than 70° (Dahm & Vagt 1977).

Both the normal-stress component $\overline{v'^2}$ and the shear-stress component $\overline{u'v'}$ were measured by means of a cross-wire probe, in the xy plane, where the 'gooseneck' part of the stem lay in a plane at approximately 90° to the flow direction. This arrangement minimizes aerodynamic interference effects. The two wires of the probe were aligned approximately at $\pm 45°$ to the flow direction, and the probe stem was inclined at 2·5° in the outer layer to account for the average upwash angle (Elsenaar & Boelsma 1974). This angle varied across the boundary layer from zero at the wall to at most 5° at the boundary-layer edge, but the present probe-driving device could not be adapted to give continuous movement in this direction. However, deviations of 2° from the true upwash angle would give rise to errors in the hot-wire signal of 4 % at most at the outer edge of the boundary layer. The projections of the wires on the xz plane were parallel to the projection of the local mean flow vector passing through the mid point between the two wire projections. For evaluation of $\overline{v'^2}$ and $\overline{u'v'}$ the following relations were used:

$$\overline{v'^2} = (1+k^2)\,(\overline{e_1' - e_2'})^2/[2K^2(1-k^2)^2], \tag{3.4}$$

and

$$\overline{u'v'} = [2K^2(1-k^2)]^{-1}\,(\overline{e_1'^2} - \overline{e_2'^2}), \tag{3.5}$$

with wires at flow angles $\alpha_{1,2} = \pm 45°$ and k approximately zero.

The measurement of the shear-stress component $\overline{v'w'}$ is more difficult than that of the other components since most hot-wire arrays need a rotatable probe stem lying in the direction of the mean velocity vector. Such a probe arrangement – as first used by Johnston (1970) – may cause aerodynamic interference effects when used in the near-wall region. To avoid this difficulty a slanted-wire probe was developed (see I). The

wire needs to be rotated into four different positions – determined by γ_2 – in order to obtain the signals necessary for the evaluation of $\overline{v'w'}$. γ_2 is the angle between the projections of the wire and the mean flow velocity vector in the xz plane. The resulting relationship is

$$\overline{v'w'} = [\overline{e'^2}_{\gamma_2=135°} - \overline{e'^2}_{\gamma_2=315°} + (\sqrt{2})^{-1}(\overline{e'^2}_{\gamma_2=0°} - \overline{e'^2}_{\gamma_2=180°})] \times 4[1-0{\cdot}25(1+k^2)]\,[K^2(1-k^2)^2\sqrt{2}]^{-1}. \quad (3.6)$$

Special emphasis was laid on keeping aerodynamic interference effects to a minimum, and for this probe they could be confined to a range of the angle of rotation γ_2 near 36°. The probe signals were therefore not affected by disturbances from the prongs at the positions needed for equation (3.6).

Finally we add some remarks in relation to the measuring accuracy which go beyond those made in I.

All probes had an active wire length of 1·3 mm, and the separation of the prongs was 4 mm. Experiments with single normal wire probes showed that the output signal for $(\overline{u'^2})^{\frac{1}{2}}/\bar{u}$ changed by up to $\pm 3\,\%$ when the active wire length was altered to 0·80 or 2·80 mm respectively. This change is typical of the near-wall region ($y \simeq 1$ mm) and results from the turbulence structure. For $y \simeq 5$ mm this effect was much less since the length scale of the turbulence is then much larger than the active wire length.

Rough estimates show that corrections to the hot-wire signals due to the high turbulence level can at most be of the order of 10 % if it is assumed that no rectification effects occur. Repeatability is better than 2 % except for the measurements of $\overline{v'w'}$. In this case differences between quantities of the same order must be calculated and an error of 1 to 2 mV in any of the four individual measurements may add up to a total error of up to $\pm 25\,\%$.

The mean-square values of the u-fluctuations between the frequencies f and $f+df$ were obtained by feeding the filtered hot-wire signals into an ADC-system which stores the digitized samples in the memory of an HP 1000 computer to which a fast Fourier transform unit (HP 5471) is attached. A software program (PSPKT) is used to manage the data flow between the different units. The terms used for the frequency domain data block are the frequency increment $\Delta f = 2$ Hz and the maximum frequency $f_{\max} = 2000$ Hz. The number of samples N in one time domain data block was 2048.

4. Discussion of measurements

A considerable amount of mean velocity and turbulence data† was accumulated during the course of this investigation and a complete presentation of all the basic data would be inappropriate. As typical examples we have therefore shown all the data along the generator $z = 0$ and selected data at the other measuring stations. Before the measurements are discussed in detail it is necessary to describe the co-ordinate system used.

The most natural and convenient co-ordinate system for experimental investigations in three-dimensional boundary layers is a right-handed, mutually orthogonal

† All data at 24 positions are given in tabulated form in the report by Fernholz *et al.* (1978).

set, the x axis of which is aligned with the direction of the mean velocity vector $\bar{u}_i$. Since the upwash angle (sometimes also called pitch angle) with respect to a generator of the cylinder was everywhere smaller than 5°, $\bar{u}_i$ was set equal to its projection in the xz plane (figure 5). Y is then the co-ordinate normal to the wall and normal to $\bar{u}_i$. The six components of the symmetrical Reynolds stress tensor were defined with respect to this co-ordinate system, the x-component u' of the fluctuating velocity lying in the direction of $\bar{u}_i$, the y-component v' normal to u' and the z-component w' normal to the plane formed by u' and v'. Figure 5 contains also additional sketches to assist the reader in his understanding of the signs and of the direction of the shear stresses $\overline{u'v'}$, $\overline{u'w'}$ and $\overline{v'w'}$.

Some of the results are presented in a cylinder-oriented co-ordinate system which is denoted by the index 'ref'. Since all the relevant angles are given, the reference values can be evaluated by applying the rules for the rotation of a co-ordinate system.

The experimental data are discussed with particular emphasis on (*a*) similarity of mean and fluctuating quantities and (*b*) on flow behaviour close to the wall.

The development of three of the most important quantities characteristic of the boundary layer in the region where three-dimensional effects become apparent is shown in figure 7. Here we have plotted the distribution of the velocity u_δ at the boundary-layer edge, of the skin friction coefficient $c_f = 2\tau_w/\rho_\delta u_\delta^2$ and of the skew angle β at a distance $y = 0{\cdot}15$ mm from the wall along three generators of the circular cylinder each 21·8 mm apart from the other, against the streamwise co-ordinate x. u_δ and c_f decrease in streamwise direction as is to be expected in an adverse pressure gradient (the excess flow escapes through the perforated outer cylinder) but they show little change in circumferential direction. Three-dimensional effects are clearly visible, however, in the distribution of β_w. The skin-friction values could not be measured further downstream since the Preston-tube pressure fell below 0·03 mm of water and the fluctuations of the signal were such that errors of $+20\,\%$ were possible. The pressure gradient parameter $\Delta = (\nu\partial p/\partial x)/(\rho u_\tau^3)$ in the region of investigation was 0·123 at most, which would suggest an error larger than 6 % according to the error range for Preston-tube measurements suggested by Patel (1965).

β at $y = 0{\cdot}15$ mm was plotted for all the measuring stations since results for this value were the closest to the wall to avoid strong wall interference on the hot wire used to determine the flow direction. Figure 6 shows the distribution of β versus y^+ in the wall region of the boundary layer and an extrapolation of the measurements to the wall. As can be seen from table 4, the difference between the flow angle measured at $y = 0{\cdot}15$ mm and the angle of the limiting streamline β_w is at most 1·9°.

As the wall is approached, figure 6 shows that there is a significant rise in the value of β below $y^+ = 20$, a fact which emphasizes further the importance of measurements in the immediate vicinity of the wall. In the figure, β then appears to fall. This sudden drop occurs consistently in most measurements shown here, but does not represent a real fall in the flow angle β. It results from curved wall effects on the response of the rotated hot wire.

An extrapolation of the skew angle β of the mean velocity $\bar{u}$ towards the wall – discarding β-values below $y^+ = 5$ – gives β_w data as shown in table 4. It is obvious from figure 6 that this is a more reliable determination of β_w than an extrapolation

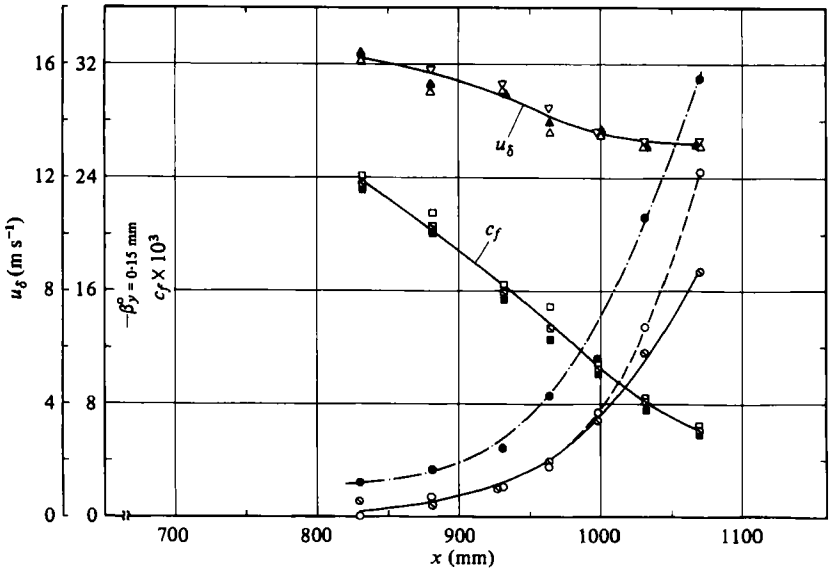

FIGURE 7. Development of the mean velocity u_δ at the boundary-layer edge, the mean flow angle β at $y = 0{\cdot}15$ mm and the skin friction coefficient c_f along three generators of the circular cylinder.

	0N01	0N02	0N03
z (mm)	−21·8	0	+21·8
$\beta_{y=0.15\mathrm{mm}}^0$	⊘	○	●
c_f	⊠	□	■
u_δ	▽	△	▲

Profile	0403	0503	0603	0703	0803	0402	0502	0602	0702	0802
$-\beta_{0.15}$	4·9	8·6	11·2	21·3	31†	2·1	3·6	7·4	13·4	24·4
$-\beta_w$	6·2	8·6	13·1	22·2	33·2	3·1	4·9	7·4	14·4	25·3

† measured at 0·20 mm.

TABLE 4

inward from the region of $y^+ = 20$–50 as is suggested in some investigations discussing differential type boundary-layer methods (cf. Johnston 1976).

We would have liked to compare the extrapolated values of β_w with records of flow visualization pictures, especially since van den Berg (1976) claims an accuracy of $\pm 0{\cdot}5°$ for β_w obtained by an oil-film method. Unfortunately this technique – and also certain others – failed, since gravity effects distorted the oil-flow pattern on the horizontal cylinder too much.

Once the flow direction has been determined, measurements of the mean velocity are straightforward except close to a wall and in a highly turbulent region (turbulent intensity larger than about 30 %). For a discussion of wall effects we refer to I.

In two-dimensional boundary layers the mean velocity in the inner region is usually made dimensionless by the skin-friction velocity u_τ and plotted versus the wall co-ordinate y^+. Measurements are then compared with a linear relationship

$$\bar{u}/u_\tau = u^+ = y^+ \tag{4.1}$$

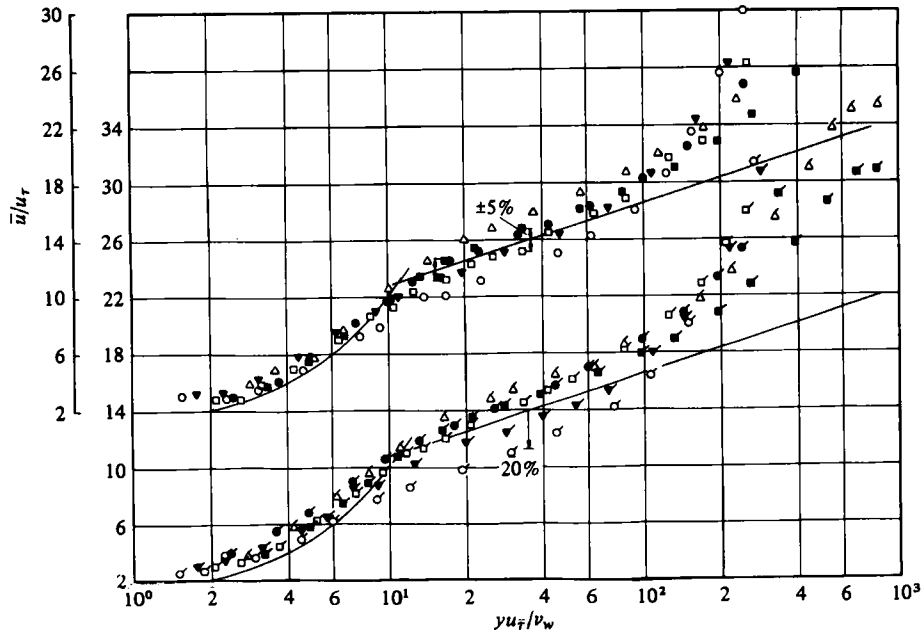

FIGURE 8. Log-law profiles in a three-dimensional turbulent boundary layer along two generators of the cylinder. The full curves correspond with equations (4.1) and (4.2) respectively. For key to symbols see table 2.

in the viscous sublayer and a logarithmic relationship

$$u^+ = (1/K)\ln(yu_\tau/\nu_w) + C, \tag{4.2}$$

where $K = 0{\cdot}40$ is the von Kármán constant and C is taken as $5{\cdot}10$.

Both semi-empirical equations are strictly valid for zero-pressure-gradient turbulent boundary layers but their validity appears to hold also for flows with adverse pressure gradients though the length of the region within which (4.2) holds then becomes considerably smaller.

An extension of these important similarity laws to three-dimensional boundary layers is of some importance but no convincing breakthrough on the theoretical side has been achieved so far in despite of some remarkable efforts such as those of East (1972) and van den Berg (1975). It is therefore useful to plot mean-velocity measurements in three-dimensional boundary layers and compare them with (4.1) and (4.2).

Figure 8 shows this comparison for the mean velocity profiles along two generators ($z = 0$ and $+0{\cdot}0218$ m) where we have plotted points using the magnitude $\bar{u}$ of the mean velocity vector $\bar{u}_i$ and the magnitude u_τ of the skin friction velocity vector $(u_\tau)_i$ as scaling velocity. Considering the errors due to the high turbulence discussed above, agreement between the measurements and the two similarity laws is surprisingly good.

The data points at the last downstream station (0802 and 0803) are low and lie below the estimated error band, mainly determined by the estimated error in skin-friction velocity of $\pm 5\%$. This is probably due to the Preston-tube measurements which are about 20% too high close to separation (cf. §3). One should note that the pressure gradient hardly influences the length of the range where measurements agree with

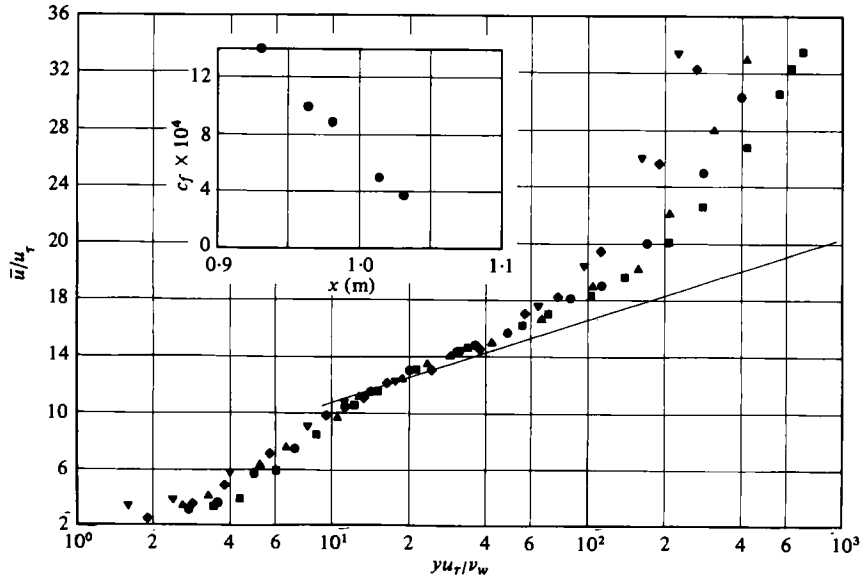

FIGURE 9. Log-law profiles along a line of symmetry in a three-dimensional boundary layer with an adverse pressure gradient. For key to symbols see table 5.

(4.2) – this seems to be different from two-dimensional boundary layers – but that its effect is large in the outer layer, as is to be expected. We have not corrected our data to account for transverse curvature effects as suggested by Bissonnette & Mellor (1974). The wall distance y would then have to be replaced by $y^* = y + y^2/2R_w$ where R_w is the radius of the inner cylinder. Such a correction does not improve agreement with (4.2) in our case, since y is very much smaller than R_w in the range of interest.

Further support for the validity of the logarithmic law in three-dimensional boundary layers is given in figure 9 where we have plotted mean velocity profiles on one of the two planes of symmetry (diverging flow) on the circular cylinder (cf. figure 4). The components of mean velocity and shear stress in the z-direction vanish at the plane of symmetry, thus making the velocity and shear-stress profiles 'locally collateral' (Nash & Patel 1972). In this case, the streamwise momentum equation reduces to its two-dimensional form, though the continuity equation does not. It is not too surprising, therefore, that, in this special case of a three-dimensional boundary layer, agreement between measurements and equations (4.1) and (4.2) is good. The velocity profiles follow the trend characteristic of an adverse pressure gradient in the streamwise direction. The same trend is shown by the increase of the shape parameter $H_{12} = \delta_1/\delta_2$, where δ_1 and δ_2, are defined by

$$\delta_1 = \int_0^\delta \left(1 - \frac{\bar{u}}{\bar{u}_\delta}\right)\left(1 + \frac{y}{R_w}\right) dy; \quad \delta_2 = \int_0^\delta \frac{\bar{u}}{u_\delta}\left(1 - \frac{\bar{u}}{u_\delta}\right)\left(1 + \frac{y}{R_w}\right) dy. \tag{4.3}$$

The key to the symbols and some important parameters for the line of symmetry flow are given in table 5 (the z-position of the line of symmetry is given in figure 4). Attention should be drawn again to the high level of turbulence which reaches maximum values as high as 68 % in the near-wall region. The normal intensity

Profile	■	●	▲	◆	▼
x (m)	0·931	0·964	0·981	1·014	1·031
H_{12}	1·64	1·79	1·85	2·05	2·25
Re_{δ_1}	5259	6267	6464	7677	7893
$[(\overline{u'^2}/\bar{u})^{\frac{1}{2}}]_{max}$	0·31	0·39	0·44	0·59	0·68

TABLE 5

profiles $\overline{u'^2}$ (not presented here) show the same behaviour as those in the fully three-dimensional boundary layer discussed below in figure 10, with the maximum closer (in terms of y^+) to the wall upstream and further away from the wall as the separation region is approached (see also Pierce & Ezekwe 1975).

Turbulence measurements

We have chosen to plot the complete data along one generator ($z = 0$) for all y positions (profiles 0N02, table 2), giving profiles for all three measuring stations along the circumference for one value of (0701–03)x only. All fluctuating quantities are presented in the mean velocity co-ordinate system, and they were made dimensionless by means of the local skin friction velocity, which we think better suited than the mean velocity $\bar{u}$ which is a function of y and x or another 'reference' velocity such as u_∞ or u_δ.

Investigating a field where relatively few data are available and where several flow-parameters may play a role, a plot of the data in dimensional co-ordinates is useful for a first inspection. We have therefore plotted the three components of the fluctuating velocity† versus the distance from the wall in figure 10. The shape of the curves is familiar from two-dimensional adverse pressure-gradient boundary layers (e.g. Bradshaw 1969). As we move in downstream direction all three components increase in magnitude and at the same time preserve their relative magnitude. The location of the maximum moves away from the wall. We cannot confirm, however, Elsenaar & Boelsma's (1974) finding that the r.m.s. values of u' and w' reach about the same value at separation.

Figure 11 shows that the values of the maxima increase markedly as we move downstream. This is mainly a result of the rapidly falling value of u_τ in the adverse pressure gradient region. Plotting the data versus y^+ gives more prominence to the near-wall data and the limits of coverage, set by the design of the hot-wire probes, are clearly visible. The u' measurements naturally extend furthest into the viscous sublayer.

For reasons of clarity and in order to facilitate comparisons with other measurements in adverse pressure gradient boundary layers (e.g. Elsenaar & Boelsma 1974, figure 27) we have plotted the Reynolds shear stresses first in dimensional co-ordinates (figure 12). Discussing $\overline{u'v'}$ first, one finds that the absolute values of the maxima increase between profiles 0202 and 0602, decrease between 0602 and 0702 and remain constant for 0702 and 0802. The location of the maximum moves away from the wall as the boundary layer proceeds into the region of the adverse pressure

† For simplicity of notation we have expressed the Reynolds stresses per unit density as is often done for flows where density is constant.

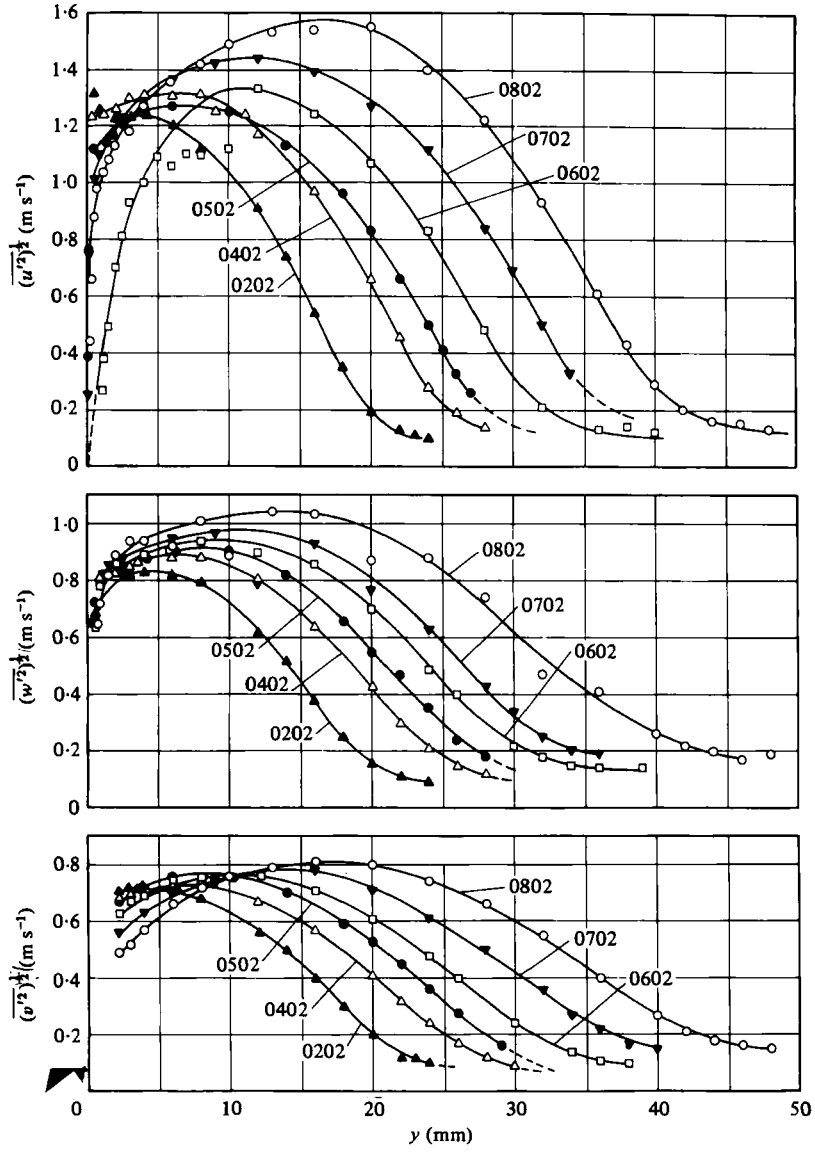

FIGURE 10. Components of fluctuating velocities across the boundary layer along the generator $z = 0$. For key to symbols see table 2.

gradient. This behaviour agrees qualitatively with that found both in three- and two-dimensional turbulent boundary layers (Bradshaw 1969; Elsenaar & Boelsma 1974) and permits the conclusion that the influence of the pressure gradient parameter dominates over three-dimensional effects as far as the $\overline{u'v'}$ distribution is concerned. Such a conclusion does not necessarily hold for the $\overline{u'w'}$ and $\overline{v'w'}$ distributions which are present only in three-dimensional flows. Both components of the Reynolds stress increase rapidly as skewing increases, $\overline{v'w'}$ finally exceeding $\overline{u'w'}$ in magnitude. As with $\overline{u'v'}$ the peaks of $\overline{u'w'}$ and $\overline{v'w'}$ shift away from the wall. Measurements in other

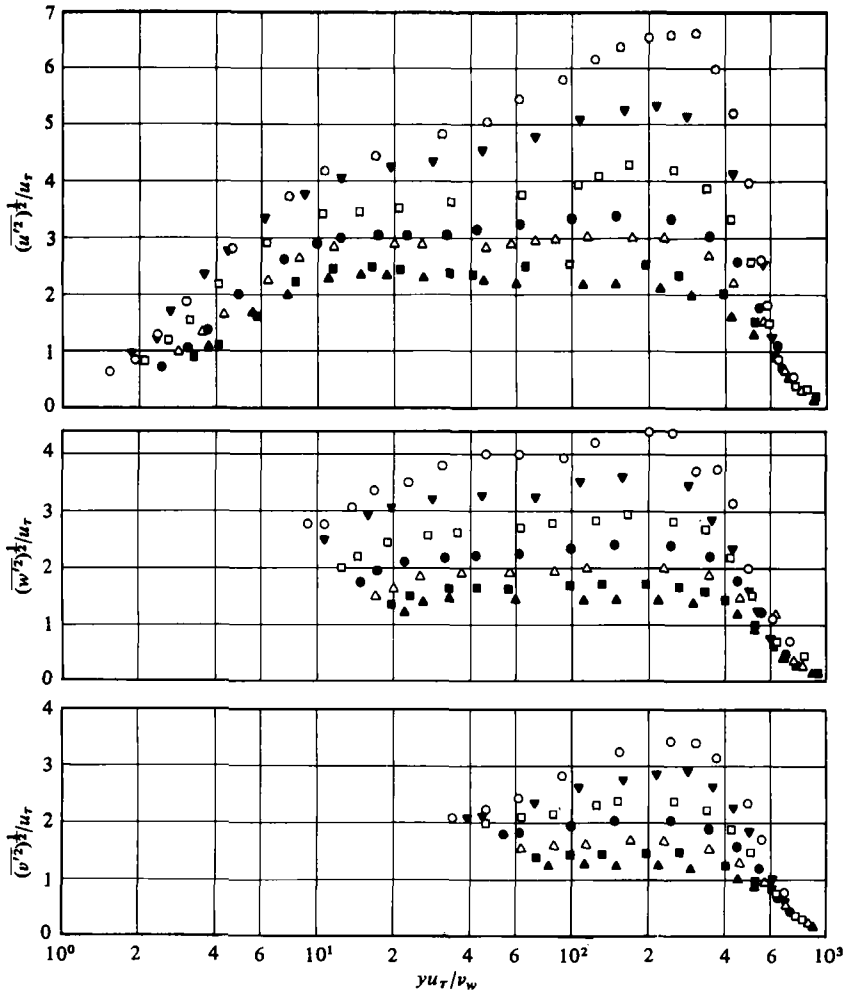

FIGURE 11. Components of dimensionless fluctuating velocities along the generator $z = 0$. For key to symbols see table 2.

experimental configurations have shown the opposite trend which is apparently a function of the boundary conditions of this specific boundary-layer flow.

Figures 13 and 14 show two Reynolds shear stress components in wall co-ordinates. As in the case of the normal components (figure 11), the level of the data is much exaggerated by the fall in u_τ. The extended scale of the abscissa in figure 14 permits to plot results at low values of y^+ in more detail and thus to show that $\overline{u'w'}$ for profiles 0603, 0702 and 0703 changes sign in the sublayer, a fact which one could not show in figure 12. We have no physical explanation for this change in sign, and, had we not come across the same phenomenon in figure 29 of Elsenaar & Boelsma's (1974) measurements, would have attributed the effect to inaccuracies of the measurement technique close to the wall.

In addition to the development of the Reynolds stresses in the streamwise direction, it was of interest to investigate whether changes of the turbulence quantities occur in the circumferential direction, caused by the pressure gradient in that direction.

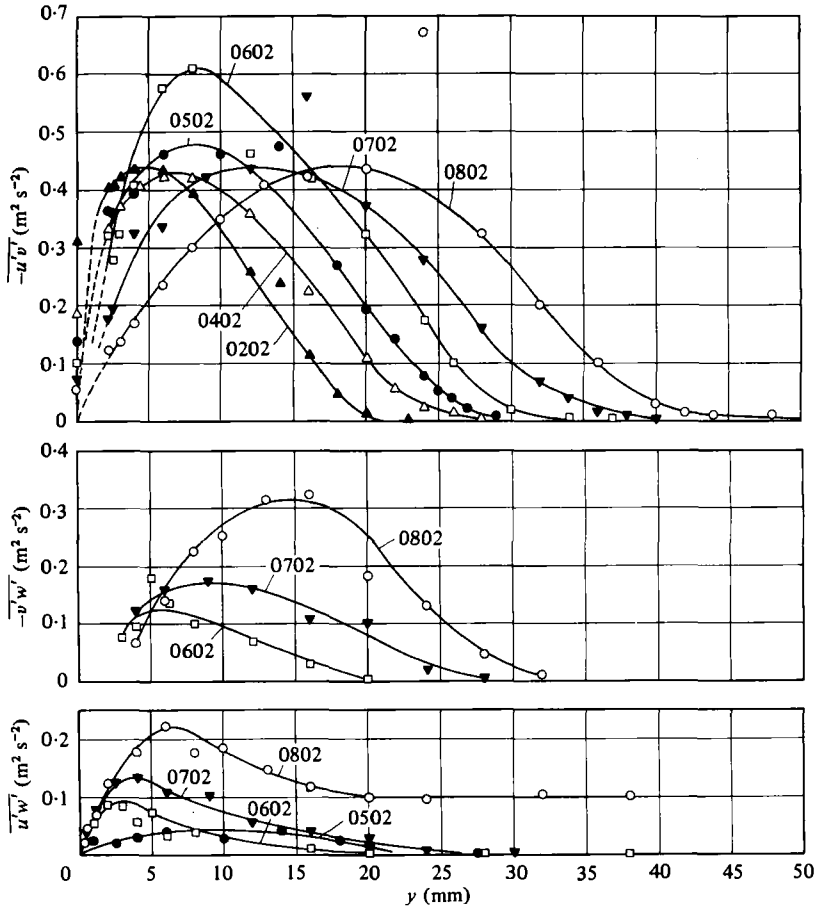

FIGURE 12. Reynolds-shear stress components along the generator $z = 0$. For key to symbols see table 2.

In figure 15 we have plotted therefore the r.m.s. values of the fluctuating velocities and the kinetic energy $\frac{1}{2}\overline{q^2}$ for profiles 0701 to 0703, i.e. at the fixed position $x = 1031$ mm. $\overline{q^2}$ is defined by $\overline{u'^2}+\overline{v'^2}+\overline{w'^2}$ and the key to the symbols is given in table 6.

From the good agreement between the profiles at the three circumferential positions we may conclude that there is no influence of the spanwise pressure gradient or of other effects due to the three-dimensionality of the flow. This three-dimensional boundary layer may therefore be called 'similar in spanwise direction' as far as the Reynolds normal stresses and consequently the kinetic energy of the fluctuating motion are concerned. If such a statement can be extended to other three-dimensional boundary layers, calculation methods which use the transport equation for the kinetic energy might be much simplified. We note here that similarity was found also for profiles 06 and 08.

Fig. 16 shows the shear stress components $\overline{u'v'}$, $\overline{v'w'}$ and the angle β of the local mean flow $\bar{u}$, the latter giving an indication of how three-dimensional effects increase from 0701 to 0703. 'Similarity in spanwise direction' can be claimed to exist for the distribution of $\overline{u'v'}$ and – to a first approximation – of $\overline{v'w'}$, the scatter between the $\overline{v'w'}$ profiles being partly due to the wider error band which had to be accepted for

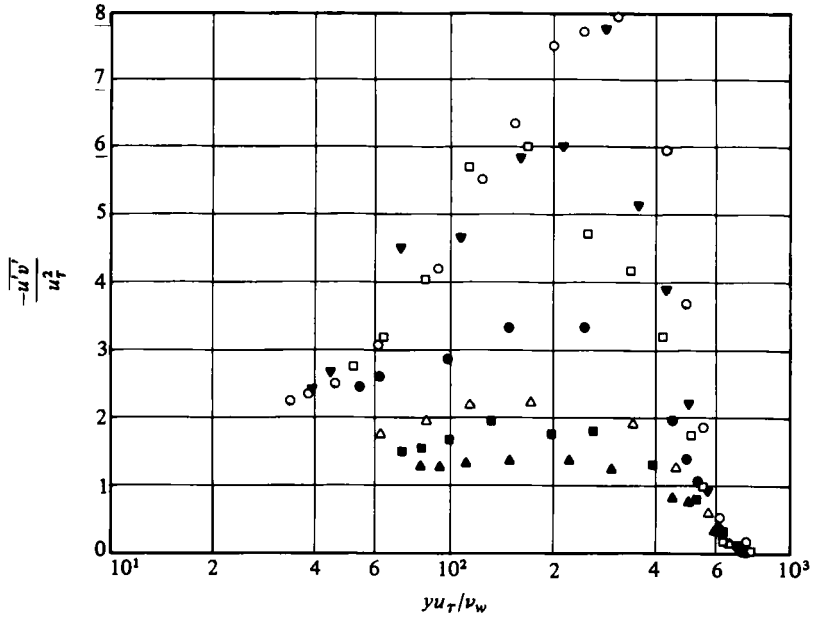

FIGURE 13. Dimensionless Reynolds-shear stress component $\overline{u'v'}$ along the generator $z = 0$. For key to symbols see table 2.

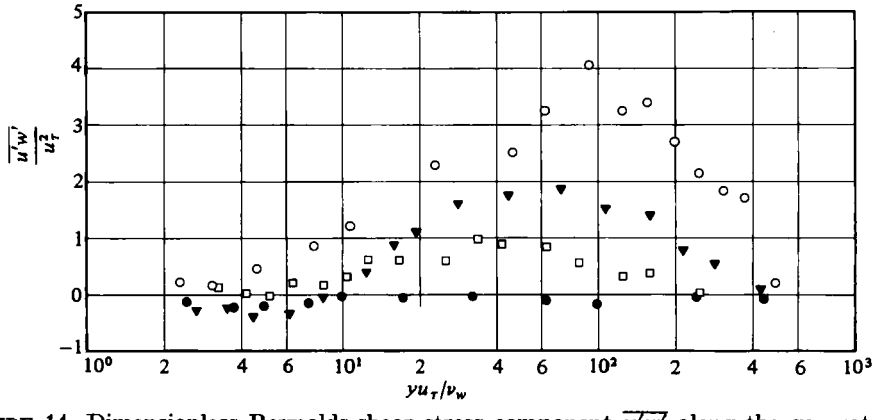

FIGURE 14. Dimensionless Reynolds-shear stress component $\overline{u'w'}$ along the generator $z = 0$. For key to symbols see table 2.

these measurements. $\overline{u'w'}$ is the Reynolds stress component which clearly does not show 'spanwise similarity'. This can be seen in figure 16 but is even more obvious in figure 17 where we have plotted $\overline{u'w'}$ profiles at positions 06, 07 and 08.

A $\overline{u'w'}$ distribution can differ therefore from a $\overline{u'v'}$ distribution in two ways, 'non-similarity in the spanwise direction' and possibly a change of sign in the near-wall region. The term $(\partial\overline{u'w'})_{\text{ref}}/\partial z$ appears in the x-component equation of motion (e.g. Nash & Patel 1972) and is usually neglected as being small compared with the remaining terms. This need not be the case in three-dimensional boundary layers close to separation as the measurements seem to show, with the consequence that it will be necessary to model also $\overline{u'w'}$ as well as $\overline{u'v'}$ and $\overline{v'w'}$ in the reference co-ordinate

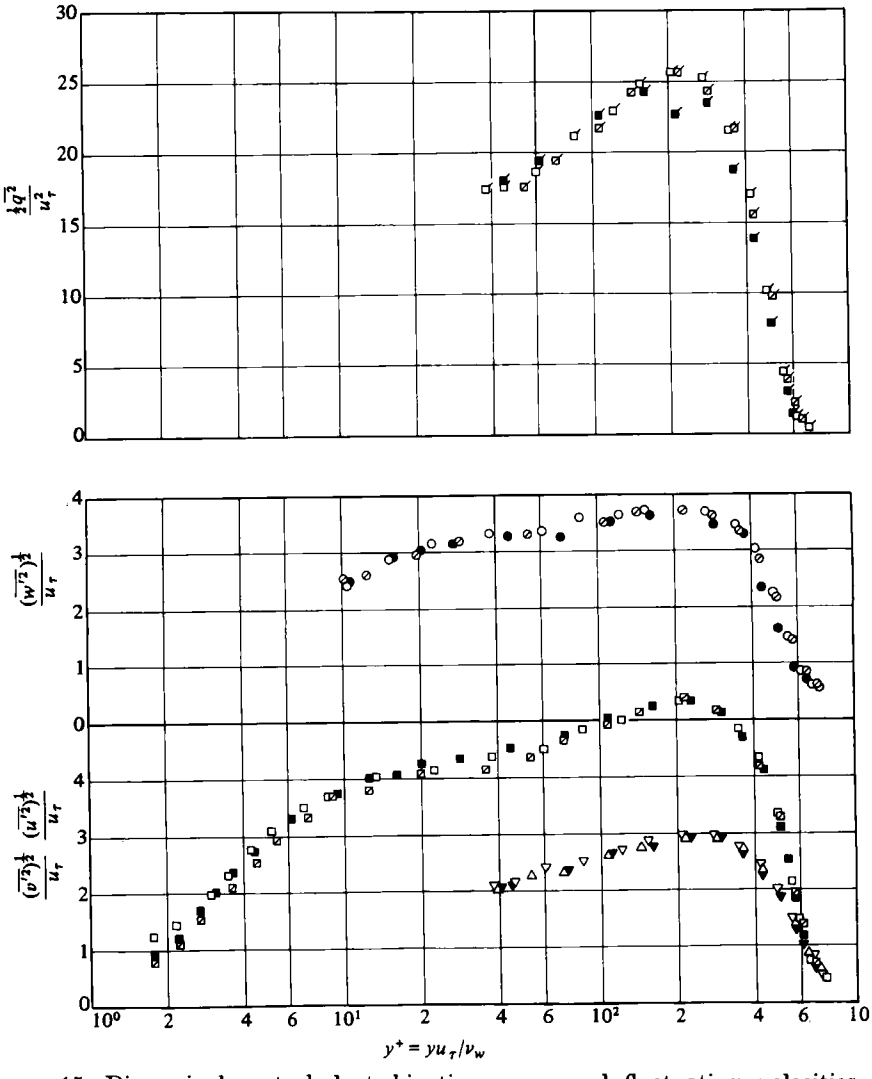

FIGURE 15. Dimensionless turbulent kinetic energy and fluctuating velocities across the boundary layer at three circumferential positions at $x = 1031$ mm. For key to symbols see table 6.

Profile	$(\overline{u'^2})^{\frac{1}{2}}$	$(\overline{v'^2})^{\frac{1}{2}}$	$(\overline{w'^2})^{\frac{1}{2}}$	$\overline{u'v'}$	$\overline{v'w'}$	$\overline{u'w'}$	$\frac{1}{2}\overline{q^2}$	$\beta°$
0701	□	▽	○	▽	◇	○	□	○
0702	■	▼	●	▼	◆	●	■	●
0703	⊠	△	⊘	△	◈	⊘	⊠	⊘

TABLE 6

system in order to solve the equations of motion. Our measurements may not provide sufficient evidence yet, but the point is one which should be taken up in any further experimental investigation, especially as Elsenaar & Boelsma (1974) showed that $\overline{u'w'}$ can reach the same magnitude as $\overline{u'v'}$ or even exceed it (Ezekwe *et al.* 1978).

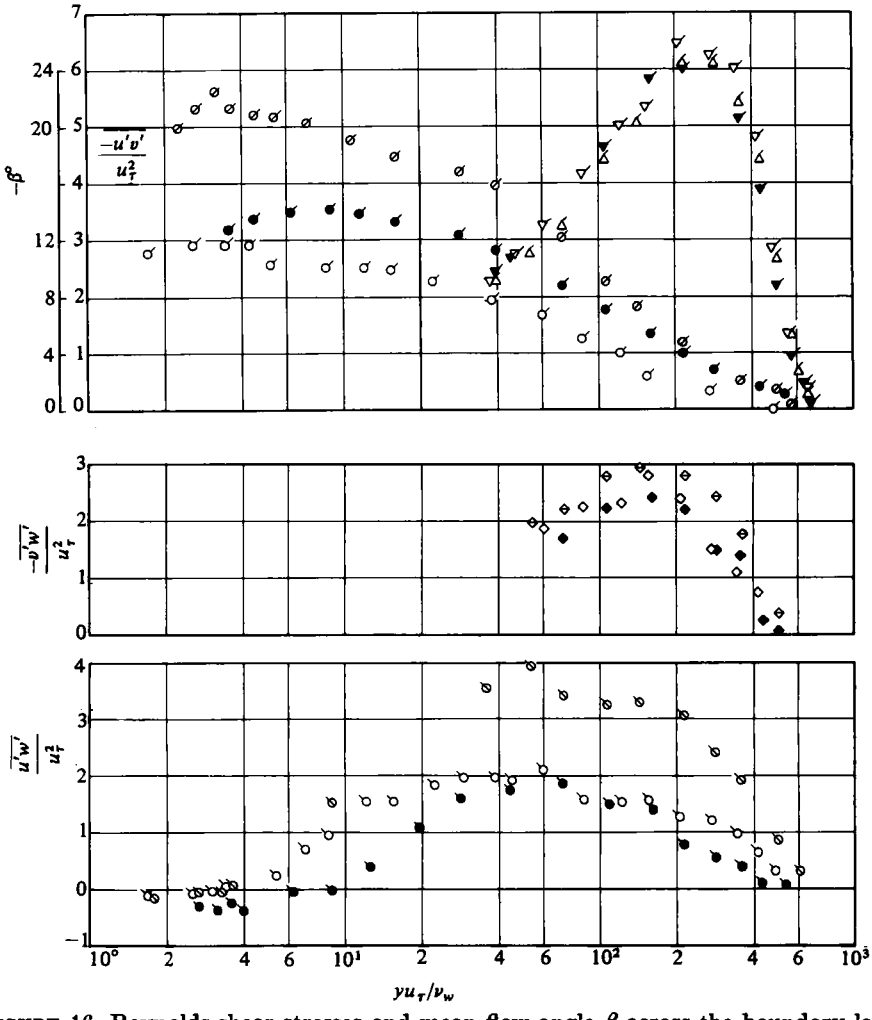

FIGURE 16. Reynolds-shear stresses and mean-flow angle β across the boundary layer at three circumferential positions at $x = 1031$ mm. For key to symbols see table 6.

Spectra

In figure 18 we have presented one-dimensional energy spectra at three positions x along the generator $z = 0$ at three distances y from the wall respectively. Symbols and some relevant data are given in table 7. Data were obtained at a position in the inner region (the smallest value of y^+), at approximately the position of the maximum for $\overline{u'v'}$ and at a position in the outer region (represented by the largest value of y^+). $\overline{u_I'^2}$ represents the integral value of $\overline{u'^2}(k)$ in the frequency range 1 Hz $\leqslant f \leqslant$ 2000 Hz and $\overline{u'^2}$ the integral value measured by the turbulence-intensity measuring device described in §2, which integrates over a frequency range 0·1 Hz $\leqslant f \leqslant 2 \times 10^4$ Hz (thus taking into account the low-frequency contributions of the spectrum). k is the wavenumber defined by $2\pi f/\bar{u}$. Since we do not know of any other spectra measurements in three-dimensional boundary layers, we have no other comparison than Klebanoff's (1955) flat plate data which are given as broken line for a qualitative

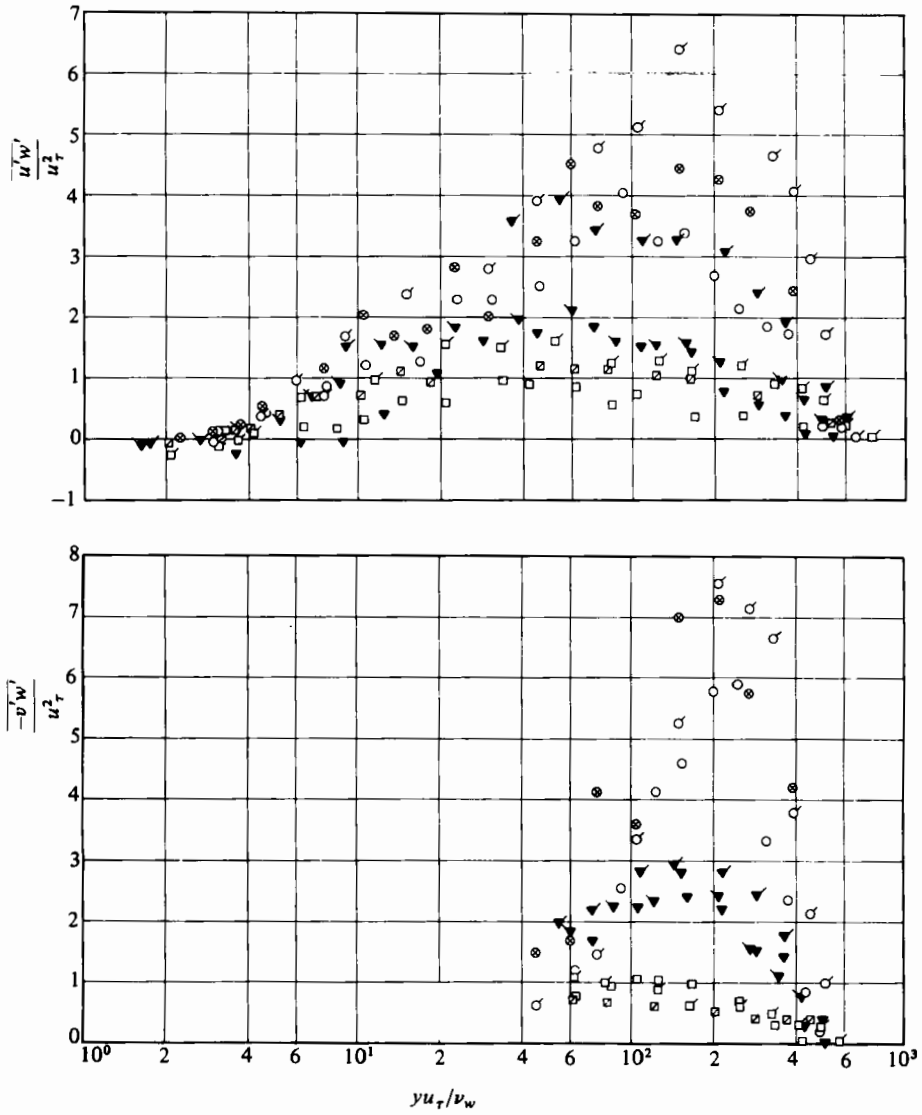

FIGURE 17. Development of Reynolds-shear stress components $\overline{u'w'}$ and $\overline{v'w'}$ in longitudinal and spanwise direction. For key to symbols see table 2.

comparison. The adverse pressure gradient spectra show the scatter 'inevitable with hot-wire measurements' (Bradshaw 1967). In the low wavenumber range the spectra of profile 0802 have the highest value compared to those of profile 0502 which is in the upstream half of the adverse pressure gradient region. Here, the spectra are dissimilar but by no means 'grossly dissimilar' as reported by Bradshaw (1967). A closer inspection of the measurements shows a surprising agreement (full line) between the data obtained in the inner region ($y^+ \approx 62$) of the various profiles, apparently independent of the pressure gradient. The uncertainty of each data point is estimated as being in the order of $\pm 5\,\%$.

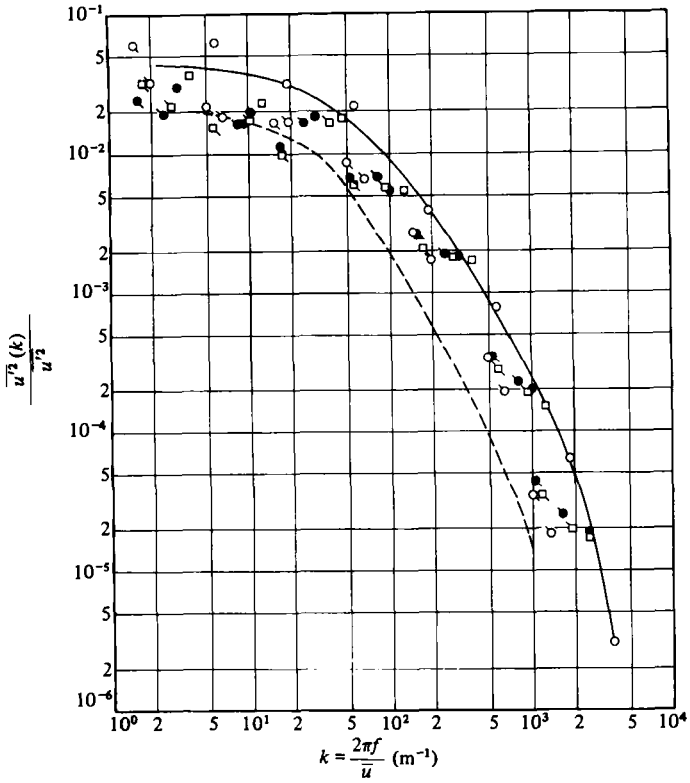

FIGURE 18. One-dimensional energy spectra in a three-dimensional boundary layer. For key to symbols see table 7.

Profile	0502			0602			0802		
Symbol	●	◑	◕	□	◱	◱	○	◔	◕
yu_τ/ν_w	61·7	148	444	62·9	167·8	420	61·6	369	555
$(\overline{u_f'^2})^{\frac{1}{2}}$ (m s^{-1})	1·326	1·453	0·983	1·356	1·594	1·077	1·388	1·788	0·470
$(\overline{u'^2})^{\frac{1}{2}}$ (m s^{-1})	1·464	1·613	0·922	1·440	1·877	1·145	1·613	1·960	0·372
$\bar{u}/u_\tau$	16·4	20·4	32	15·8	20·8	35·1	14·2	40·8	53·8

TABLE 7

5. Discussion of results

Basing our arguments on the measurements presented in §4 and the improved measuring techniques discussed in I we now comment on some of the still unsettled questions in three-dimensional boundary layers as pointed out by Pierce, Tennant & Rule (1976) and by Johnston (1976).

5.1. *Existence and limits of near-wall similarity in three-dimensional turbulent boundary layers*

The controversy about similarity laws and their constants in the inner region of a two-dimensional boundary layer has more or less abated, and the linear and logarithmic

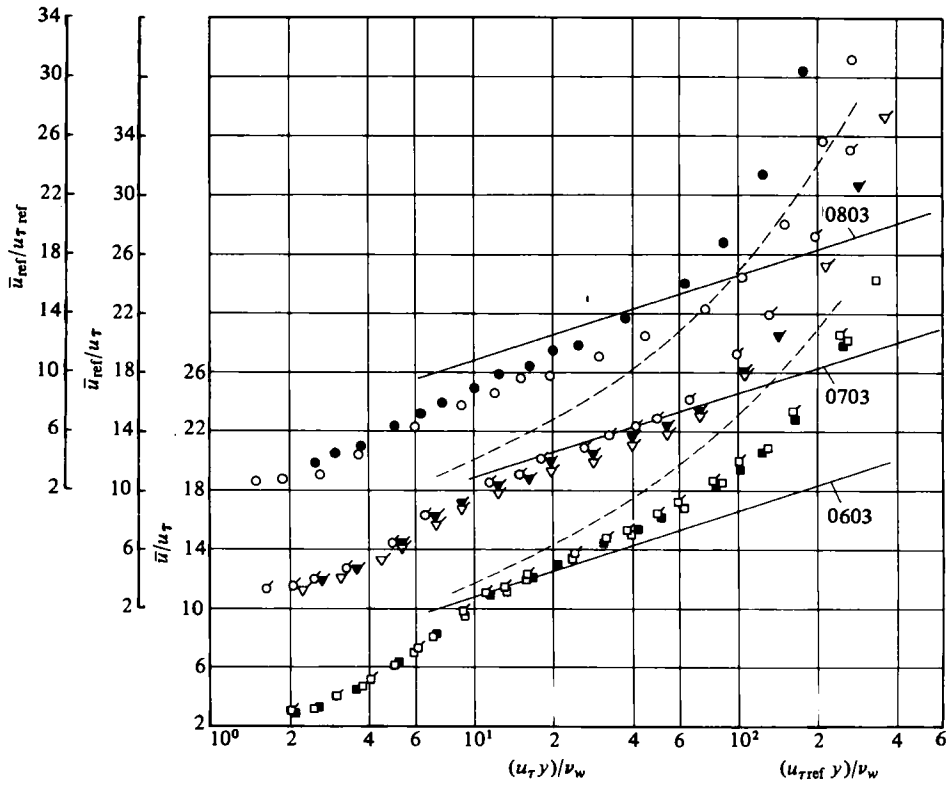

FIGURE 19. Log-law profiles for various combinations of magnitude and components of the skin-friction and mean-velocity vector (--- van den Berg 1975). □, ○, ●, $\bar{u}_{ref}/u_{\tau ref}$; □, ▽, $\bar{u}_{ref}/u_\tau$; ■, ▼, ○, u/u_τ.

laws (equations 4.1 and 4.2) for the velocity distribution are well established. The experimental evidence for these relationships is plentiful and of high quality in incompressible boundary layers with zero-pressure gradient and covers a wide range of Reynolds numbers ($5\times10^2 \leqslant Re_{\delta_2} \leqslant 3\times10^5$). A comparison between measurements and the various log-law concepts in three-dimensional boundary layers is not straightforward as opinions differ as to whether the magnitude or some component of the mean velocity and/or the skin friction vector should be used when plotting the law of the wall. East (1974) suggested, besides the magnitude $\bar{u}$ of the mean velocity vector $\bar{u}_i$, the velocity $\bar{u}^* = \bar{u}_{ref} \sec\beta_w$ where $\bar{u}_{ref}$ is the velocity component in the direction of the external streamline ($\bar{u}_{ref} = |\bar{u}_i| \cos\beta$) and β_w is the cross-flow angle at the wall, and van den Berg (1976) used $\bar{u}_{ref}$. Only two suggestions were made for the appropriate skin friction velocity, the magnitude u_τ of the skin friction vector $(u_\tau)_i$ or the component, $u_{\tau ref} = u_\tau \cos\beta$. Figure 19 therefore shows $(\bar{u}_{ref}/u_{\tau ref})$ plotted against $y u_{\tau ref}/\nu_w$ and $\bar{u}_{ref}/u_\tau$, $\bar{u}/u_\tau$ against $u_\tau y/\nu_w$ for profiles 0603, 0703 and 0803. A comparison of some experimental data is made with the semi-empirical relations (4.2) (full line) and (5.1) (broken line). The latter equation represents van den Berg's (1975) law of the wall for the component $\bar{u}_{ref}/u_\tau$:

$$\bar{u}_{ref}/u_\tau = k^{-1}[\ln y^+ + A + 0{\cdot}5\alpha_x y^+ + 0{\cdot}5\beta_x (\ln y^+)^2 y^+ k^{-2}], \tag{5.1}$$

where $k = 0{\cdot}40$, $A = 2$, $y^+ = u_\tau y/\nu$, $\alpha_x = \nu(dp/dx)/\rho u_\tau^3$

and $$\beta_x = \nu(du_\tau/dx)/u_\tau.$$

The various plots have no great influence on the appearance of the results, but, in all cases, large discrepancies can be seen between the data and equation (5.1) which supposedly takes into account both pressure gradient and inertial forces. Good agreement between any law at the wall and measurements would enable users of some available numerical methods for three-dimensional boundary layers to start their computations further away from the wall and thus save computing time. Considering the evidence in figures 8 and 19, we agree with Prahlad's (1972) and Pierce & Zimmerman's (1973) conclusion that the law of the wall for two-dimensional boundary layers is valid in three-dimensional boundary layers of moderate (we extend this to strong) adverse pressure gradients and that the two-layer hypothesis viscous sublayer and log-law region, is applicable also to three-dimensional boundary layers. We may add, however, a word of caution here. The three-dimensional boundary layer investigated in our experiment had a strong adverse pressure gradient in the direction of the outer flow and a weak circumferential pressure gradient. It is possible, therefore, that a stronger circumferential pressure gradient may affect the flow differently and thus invalidate the above statement.

Our measurements show also that the magnitude of the mean velocity vector in the viscous sublayer follows a linear relationship as in two-dimensional boundary layers, even when the boundary layer is close to separation (for weaker pressure gradients the same results were found by Pierce & Krommenhoek (1968), East (1974) and Hebbar & Melnik (1978).

5.2. *Skewed and collateral velocity profiles in the near-wall region*

Another controversy in the literature has been whether the mean velocity profile in the near-wall region of a three-dimensional boundary layer, generated by a pressure gradient transverse to the direction of the streamlines in the main flow, is collateral or skewed. Pierce *et al.* (1976) pointed out that the existence of a collateral boundary layer is inconsistent with the governing equations and that no near-wall collateral flow was predicted by their analysis (Pierce & East 1972). These theoretical results are backed by the experimental investigations of Rogers & Head (1969), Vermeulen (1971) and in general Elsenaar & Boelsma (1974) – the latter authors showing some velocity profiles with collateral regions close to the wall – and opposed by the experiments of Hebbar & Melnik (1978), for example. For a list of other investigations where near-wall collateral velocity profiles were found, the reader is referred to Pierce & East (1972). The present authors hope to have clarified experimentally in I some of the measuring problems connected with flow angle measurements in the near-wall region of a three-dimensional boundary layer, such as aerodynamic interference effects of the probes, high levels of turbulence or heat sink effects of the wall. Due to the geometry of our test section, we could not use the technique which employs a hot wire held parallel to the wall on prongs entering the flow through a rotatable wall plug as applied in all the experiments mentioned above, though with different types of probes. This would have been necessary to solve the contradiction between the collateral velocity profiles found by Hebbar & Melnik (1978) and the skewed velocity profiles with a monotonic increase of the flow angle towards the wall given in the other investigations. We do find, however, more evidence for skewed mean-velocity

profiles and would like to see at least all measurements of flow angle by yaw-tube probes or inclined hot-wire probes carefully checked for aerodynamic interference and wall interference effects.

5.3. *Directions of turbulent shear stress, resultant velocity gradient, and mean velocity*

Apart from the generation of the $\overline{u'w'}$ and $\overline{v'w'}$ components one of the main effects of three-dimensionality on the turbulence is that the direction of the resultant turbulent shear stress is not the same as the direction of the resultant velocity gradient. This difference in direction was first recognized by Bradshaw & Terrell (1969) who drew attention to the contradiction lying in isotropic eddy viscosity models often used in computation methods.

The skew angle γ of the Reynolds shear stress vector is defined as the angle between the projections of this vector and the direction of the streamline at the boundary-layer edge on the wall. It was calculated according to equation (5.2)

$$\gamma = \tan^{-1}(\overline{v'w'}/\overline{u'v'}) + \beta, \tag{5.2}$$

where β is the skew angle of the mean velocity vector (figure 5). The skew angle of the resultant velocity gradient or 'mean shear' as measured from the direction of the streamline at the boundary-layer edge is given by

$$\zeta = \tan^{-1}\left(\frac{\partial \bar{w}_{\mathrm{ref}}/\partial y}{\partial u_{\mathrm{ref}}/\partial y}\right), \tag{5.3}$$

where $\bar{u}_{\mathrm{ref}} = \bar{u}\cos\beta$ and $\bar{w}_{\mathrm{ref}} = \bar{u}\sin\beta$.

The angles β, γ and ζ of profiles 0602, 0702 and 0802 are shown in figures 20 and 21. The cross-flow angle β is of opposite sign to the angles γ and ζ except close to the wall where β and ζ converge to the same limiting value. γ cannot be determined in the vicinity of the wall since measurements of $\overline{v'w'}$ and $\overline{u'v'}$ cannot be performed there due to the probe geometry. However, a fall of γ in the wall region of profiles 0702 and 0802 indicates at least the direction of γ which at the wall should be the same as that of velocity and velocity gradient (Bradshaw & Terrell 1969).

Johnston (1976) pointed out that two different situations might occur, one where the skew angle of the shear stress vector γ lags the angle of the mean velocity gradient ζ (cf., for example, Bradshaw & Terrell 1969, Elsenaar & Boelsma 1974) and the other where γ leads ζ (Pierce & Ezekwe 1975). The present measurements apparently belong to the second group, with the 'lead effect' increasing with growing three-dimensionality up to 30° which is three times as much as the often observed 10°. Following the argument put forward by Johnston (1976) this behaviour indicates an anti-history effect or in other words a lack of time for the mean velocity gradient to follow the turbulence structure which has been changed severely by the adverse pressure gradient and the three-dimesnional effects over a comparatively short distance. This order of events cannot yet be explained. All three angles tend to zero at the outer edge of the boundary layer though it is sometimes difficult to have well defined values of ζ close to the edge of the boundary layer (e.g. 0602).

Our measurements strengthen the argument that the lag between the angles ζ and γ is by no means unique but they do not yet provide enough physical insight as to the

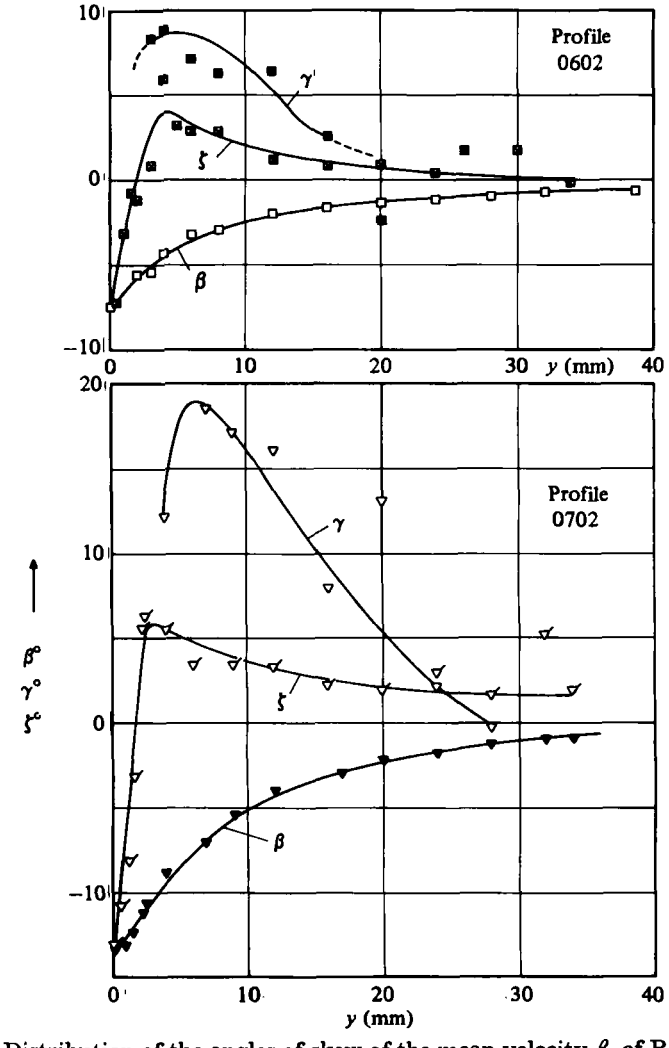

FIGURE 20. Distribution of the angles of skew of the mean velocity β, of Reynolds shear stress γ and of mean shear ζ (profiles 0602, 0702).

controlling parameters of this phenomenon, so that more experiments are needed to establish a correlation between the direction of the shear-stress vector and the vector of the mean velocity gradient.

5.4. *The ratio of turbulent shear stress and turbulent kinetic energy*

While investigating a two-dimensional turbulent boundary layer with zero pressure gradient Klebanoff (1955) introduced the ratio $2a_1$ of the turbulent shear stress $\overline{u'v'}$ to the kinetic energy of the turbulent fluctuations $\frac{1}{2}\overline{q^2} = 0{\cdot}5(\overline{u'^2}+\overline{u'^2}+\overline{w'^2})$ which was later used by Bradshaw (1971) as one of the semi-empirical inputs ($a_1 = 0{\cdot}15$) for his calculation method for turbulent boundary layers. If the pressure gradient effect is zero or still weak, a_1 is close to 0·15 as can be seen from figure 22(*a*) where we have plotted the ratio $2\overline{u'v'}/\overline{q^2}$ for velocity profiles in the upstream region of our

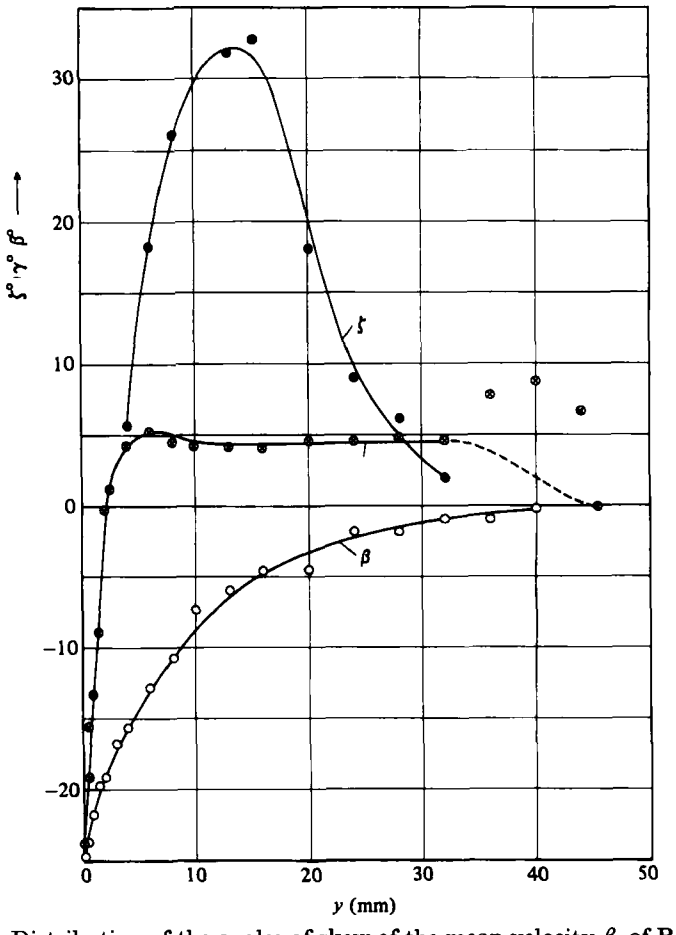

FIGURE 21. Distribution of the angles of skew of the mean velocity β, of Reynolds shear stress γ and of mean shear ζ (profile 0802).

boundary layer (02–04). Further downstream, with effects of adverse pressure gradient and three-dimensionality becoming stronger, a_1 is no longer constant but increases by a factor of about 3 from the inner region towards the edge of the boundary layer with a limiting value again of 0·15 for a_1 (figure 22*b*). In the three-dimensional boundary layer the turbulent shear stress τ_t consists of the components $\overline{u'v'}$ and $\overline{v'w'}$ and we have plotted $2\tau_t/\overline{q^2}$ in figure 22(*c*). Apart from profile 0603, the same tendency prevails as in figure 22(*b*), i.e. a_1 cannot be considered as a constant value across the boundary layer. This result differs from Elsenaar & Boelsma's (1974) finding that a_1 is more or less constant across the layer but that its value is lower and lies between 0·11 and 0·13. This means that the magnitude of the turbulent shear stress in the three-dimensional boundary layer is lower than in the two-dimensional boundary layer when scaled by the local turbulent kinetic energy.

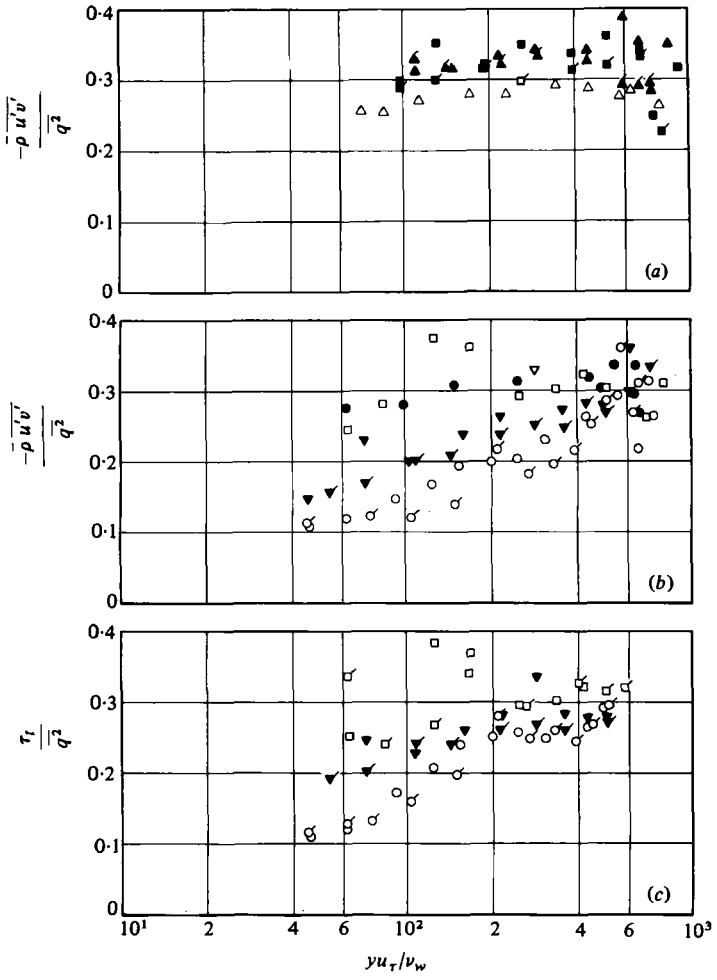

FIGURE 22. Ratio of shear stress and kinetic energy across a three-dimensional boundary layer. For key to symbols see table 2.

We are grateful to B. Dziomba and P. Dengel for their assistance with the measurements, to C. Mohr for the data computation and to Dr P. J. Finley and Professor P. Bradshaw for helpful discussions.

REFERENCES

BERG, B. VAN DEN 1975 A three-dimensional law of the wall for turbulent shear flows. *J. Fluid Mech.* **70**, 149–160.

BERG, B. VAN DEN 1976 Investigations of three-dimensional incompressible turbulent boundary layers. *NLR Tech. Rep.* 76001 U.

BISSONNETTE, L. R. & MELLOR, G. L. 1974 Experiments on the behaviour of an axisymmetric turbulent boundary layer with a sudden circumferential strain. *J. Fluid Mech.* **63**, 369–413.

BRADSHAW, P. 1967 'Inactive' motion and pressure fluctuations in turbulent boundary layers. *J. Fluid Mech.* **30**, 241–258.

BRADSHAW, P. 1969 The response of a constant-pressure turbulent boundary layer to the sudden application of an adverse pressure gradient. *Aero. Res. Counc. R & M.* 3575.

BRADSHAW, P. 1971 Calculation of three-dimensional turbulent boundary layers. *J. Fluid Mech.* **46**, 417–445.

BRADSHAW, P. & TERRELL, M. G. 1969 The response of a turbulent boundary layer on an 'infinite' swept wing to the sudden removal of pressure gradient. *NPL Aero Rep.* 1305.

COMTE-BELLOT, G., STROHL, A. & ALCARAZ, E. 1971 On aerodynamic disturbances caused by single hot-wire probes. *Trans. A.S.M.E.* E, *J. Appl. Mech.* **93**, 767–774.

DAHM, A. & VAGT, J.-D. 1977 Entwicklung und Herstellung interferenzarmer Hitzdrahtsonden. *HFI INst.* 01/77.

DEAN, R. C. 1953 *Aerodynamic Measurements.* Gas Turbine Laboratory, M.I.T.

DECHOW, R. 1977 Mittlere Geschwindigkeit und Reynoldsscher Spannungstensor in der dreidimensionalen turbulenten Wandgrenzschicht vor einem stehenden Zylinder. Dissertation Universität Karlsruhe. Strömungsmaschinen u. Strömungsmechanik Heft 21.

EAST, L. F. 1972 A prediction of the law of the wall in compressible three-dimensional turbulent boundary layers. *RAE Tech. Rep.* **72**, 178.

EAST, L. F. 1974 Measurements of the three-dimensional incompressible turbulent boundary layer induced on the surface of a slender delta wing by the leading edge vortex. *RAE Tech. Rep.* **73**, 141.

EICHELBRENNER, E. A. 1973 Three-dimensional boundary layers. *Ann. Rev. Fluid Mech.* **5**, 339–360.

ELSENAAR, A. & BOELSMA, S. H. 1974 Measurements of the Reynolds stress tensor in a three-dimensional turbulent boundary layer under infinite swept wing conditions. *NLR Tech. Rep.* 74095 U.

EZEKWE, C. I., PIERCE, F. J. & MCALLISTER, J. E. 1978 Measured Reynolds stress tensor in a three-dimensional turbulent boundary layer. *A.I.A.A. J.* **16**, 645–647.

FANNELØP, T. K. & KROGSTAD, P. A. 1975 Three-dimensional turbulent boundary layers in external flows: a report on Euromech 60. *J. Fluid Mech.* **71**, 815–826.

FERNHOLZ, H. H. & VAGT, J.-D. 1977 Measurements in an axisymmetric turbulent boundary layer with weak and strong three-dimensional disturbances. In *Structure and Mechanisms of Turbulence I*, Lecture Notes in Physics, vol. 75, (ed. H. Fielder), pp. 222–233. Springer.

FERNHOLZ, H. H., VAGT, J.-D., DZIOMBA, B. & DENGEL, P. 1978 Messungen in einer dreidimensionalen turbulenten Wandgrenzschicht an einer gekrümmten Wand. *HFI Institutsbericht* 01/78. (2. ergänzte Auflage 1980). Technische Universität Berlin.

FROEBEL, E. & VAGT, J.-D. 1974 Ein automatisch abgleichendes Flüssigkeitsmanometer mit digitaler Anzeige. *DLR-FB* 74–40.

FROEBEL, E. & VAGT, J.-D. 1977 Meß- und Auswerteverfahren von Hitzdrahtsignalen mit dem Turbulenzgradmesser TGM III der DFVLR. *DLR-FB* 77–61.

GRANDE, G. DE & HIRSCH, CH. 1978 Three-dimensional incompressible turbulent boundary layers. *Int. Rep. Vrije Univ. Brussels* STR-8.

HEBBAR, K. S. & MELNIK, W. L. 1976 Measurements in the near-wall region of a relaxing three-dimensional low speed turbulent air boundary layer. *Univ. Maryland, Tech. Rep.* AE-76-1.

HEBBAR, K. S. & MELNIK, W. L. 1978 Wall region of a relaxing three-dimensional incompressible turbulent boundary layer. *J. Fluid Mech.* **85**, 33–56.

JOHNSTON, J. P. 1970 Measurements in a three-dimensional turbulent boundary layer induced by a swept forward-facing step. *J. Fluid Mech.* **42**, 823–844.

JOHNSTON, J. P. 1976 Experimental studies in three-dimensional turbulent boundary layers. *Stanford Univ. Thermosciences Div. Rep.* MD-34.

KLEBANOFF, P. S. 1955 Characteristics of turbulence in a boundary layer with zero pressure gradient. *N.A.C.A. Rep.* 1247.

KRAUSE, E. & KORDULLA, W. 1975 Investigation of three-dimensional boundary layers on swept wings. Paper presented at Euromech 60, Trondheim.

MCCROSKEY, W. J. & DURBIN, E. J. 1972 Flow angle and shear stress measurements using heated films and wires. *Trans. A.S.M.E.* I, *J. Basic Engng.* **94**, 46–52.

MÜLLER, U. 1979 Messung von Reynoldsschen Spannungen und zeitlich gemittelten Ge schwindigkeiten in einer drei-dimensionalen Grenzschicht mit nichtverschwindendem Druckgradienten. Dissertation RWTH Aachen.

NASH, J. F. & PATEL, V. C. 1972 *Three-Dimensional Turbulent Boundary Layers.* SBC Technical Books.

PATEL, V. C. 1965 Calibration of the Preston tube and limitations on its use in pressure gradients. *J. Fluid Mech.* **23**, 185–208.

PIERCE, F. J. & EAST, J. L. 1972 Near-wall collateral flow in three-dimensional turbulent boundary layers. *A.I.A.A. J.* **10**, 334–336.

PIERCE, F. J. & EZEKWE, C. I. 1975 Turbulent stress tensors in a three-dimensional boundary layer. *Virginia Polytech. Inst. Rep.* E-75-1.

PIERCE, F. J. & KROMMENHOEK, D. H. 1968 Wall shear stress diagnostics in three dimensional turbulent boundary layers. *Virginia Polytech. Mech. Engng. Dept, Interim Tech. Rep.* no. 2.

PIERCE, F. J., TENNANT, M. H. & RULE, J. A. 1976 Near-wall similarity in three-dimensional turbulent flows – Experimental system. *Virginia Polytech. Inst. Rep.* E-76-16.

PIERCE, F. J. & ZIMMERMAN, B. B. 1973 Wall shear stress interference from two- and three-dimensional turbulent boundary layer velocity profiles. *Trans. A.S.M.E.* I, *J. Fluids Engng.* **95**, 61–67.

PRAHLAD, T. S. 1972 Mean velocity profiles in three-dimensional incompressible turbulent boundary layers. *A.I.A.A.J.* **11**, 359–365.

ROGERS, B. K. & HEAD, M. R. 1969 Measurements of three-dimensional boundary layers. *J. Roy. Aeronaut. Soc.* **73**, 796–798.

SWAMY CHANDRASEKHARA, N. V., GOWDA LAKSHMANA, B. H. & LAKSHMINATH, V. R. 1978 Turbulence measurements in the three-dimensional boundary layer on a yawed flat plate at incidence. *Z.F.W.* **2**, 15–22.

VAGT, J.-D. 1973 Bemerkungen zur Auslegung eines Unterschall-Freistrahl Windkanals. *Z.f.W.* **5**, 159–162.

VAGT, J.-D. 1979 Hot-wire probes in low speed flow. *Prog. Aerospace Sci.* **18**, 271–323.

VAGT, J.-D. & FERNHOLZ, H. H. 1973 Use of surface fences to measure wall shear stress in three-dimensional boundary layers. *Aero. Quart.* **24**, 87–91.

VAGT, J.-D. & FERNHOLZ, H. H. 1977 Wall interference effects of static pressure probes in an incompressible turbulent boundary layer. *Aero. Quart.* **28**, 176–184.

VAGT, J.-D. & FERNHOLZ, H. H. 1979 A discussion of probe effects and improved measuring techniques in the near wall region of an incompressible three-dimensional turbulent boundary layer. *AGARD Conf. Proceedings.* 271.

VERMEULEN, A. J. 1971 Measurements of three-dimensional turbulent boundary layers. Ph.D. thesis, University of Cambridge.